Cell

Transit-Amplifying Cells Orchestrate Stem Cell Activity and Tissue Regeneration

Ya-Chieh Hsu,[1] Lishi Li,[1] and Elaine Fuchs[1,*]
[1]Howard Hughes Medical Institute, Laboratory of Mammalian Cell Biology and Development, The Rockefeller University, 1230 York Avenue, New York, NY 10065, USA
*Correspondence: fuchslb@rockefeller.edu
http://dx.doi.org/10.1016/j.cell.2014.02.057

SUMMARY

Transit-amplifying cells (TACs) are an early intermediate in tissue regeneration. Here, using hair follicles (HFs) as a paradigm, we show that emerging TACs constitute a signaling center that orchestrates tissue growth. Whereas primed stem cells (SCs) generate TACs, quiescent SCs only proliferate after TACs form and begin expressing Sonic Hedgehog (SHH). TAC generation is independent of autocrine SHH, but the TAC pool wanes if they can't produce SHH. We trace this paradox to two direct actions of SHH: promoting quiescent-SC proliferation and regulating dermal factors that stoke TAC expansion. Ingrained within quiescent SCs' special sensitivity to SHH signaling is their high expression of GAS1. Without sufficient input from quiescent SCs, replenishment of primed SCs for the next hair cycle is compromised, delaying regeneration and eventually leading to regeneration failure. Our findings unveil TACs as transient but indispensable integrators of SC niche components and reveal an intriguing interdependency of primed and quiescent SC populations on tissue regeneration.

INTRODUCTION

The ability to make tissue(s) is a necessary feature of stem cells (SCs). Some SCs, such as those of the intestinal epithelium, hematopoietic system, or epidermis, continually generate tissues throughout life. Others, such as those of mammary glands or hair follicles (HFs), undergo less frequent and periodic bouts of regeneration. Regardless of these differences, SC proliferation is tightly regulated to suit the homeostatic needs of their respective tissues, and disruption of this regulation can lead to severe consequences. For example, mutations causing hematopoietic stem cells (HSCs) to hyperproliferate often lead to their exhaustion (Pietras et al., 2011; Yilmaz et al., 2006), whereas mutations causing insufficient SC activity in HFs results in a failure to regrow the hair coat after rounds of regeneration (Chen et al., 2012). Elucidating how SC proliferation is governed and delineating the impact of niche components on this process therefore become critical.

Historically, SCs are thought to receive their regulatory cues from neighboring heterologous cells within a defined local microenvironment, referred to as the SC niche (Morrison and Spradling, 2008). Recent studies suggest that some differentiated progeny of SCs can also be niche components and provide feedback regulation to their SC parents (Hsu and Fuchs, 2012). For example, in the HF, committed SCs return to the niche, where they form an inner bulge layer of differentiated Keratin6$^+$ (K6$^+$) progeny that inhibits the activation of SCs in the outer bulge layer (Hsu et al., 2011). In the intestinal SC niche, terminally differentiated Paneth cells sandwiched between crypt SCs promote SC self-renewal (Sato et al., 2011). In the hematopoietic system, differentiated macrophages home back to the bone marrow, where they enforce HSC retention and restrict their movement into the bloodstream (Chow et al., 2011; Winkler et al., 2010). In *Drosophila*, differentiating hemocytes provide inhibitory cues to maintain quiescence in their hematopoietic progenitor parents (Mondal et al., 2011), and in ovary, signals from specialized progeny, polar cells, influence the functions of follicular SCs (Vied et al., 2012). Altogether, the lineage feedback circuitry that has emerged thus far involves terminally differentiated SC progeny that act locally within the niche.

Transit-amplifying cells (TACs) are an undifferentiated population in transition between SCs and differentiated cells. Although feedback circuitry between TACs and SCs has not been described, several aspects of tissue regeneration suggest that such communication would be beneficial for balancing the process. Although proliferation of SCs initiates tissue regeneration, formation of the TAC pool represents a bottleneck step in the process: once TACs are formed, tissue regeneration proceeds with no return. Feedback regulation from TACs might instruct SCs to further replenish downstream lineages and coordinate the self-renewal of SCs during regeneration. In addition, as the major driving force for tissue production, TACs may signal to heterologous cell types to stage an optimal environment for generating tissue. Although attractive, evidence in support of such roles is lacking.

The mouse HF is an ideal system to explore possible communication between SCs and TACs. Each HF cycles between an active phase of tissue production (anagen), destruction (catagen), and rest (telogen) (Müller-Röver et al., 2001; Plikus and Chuong,

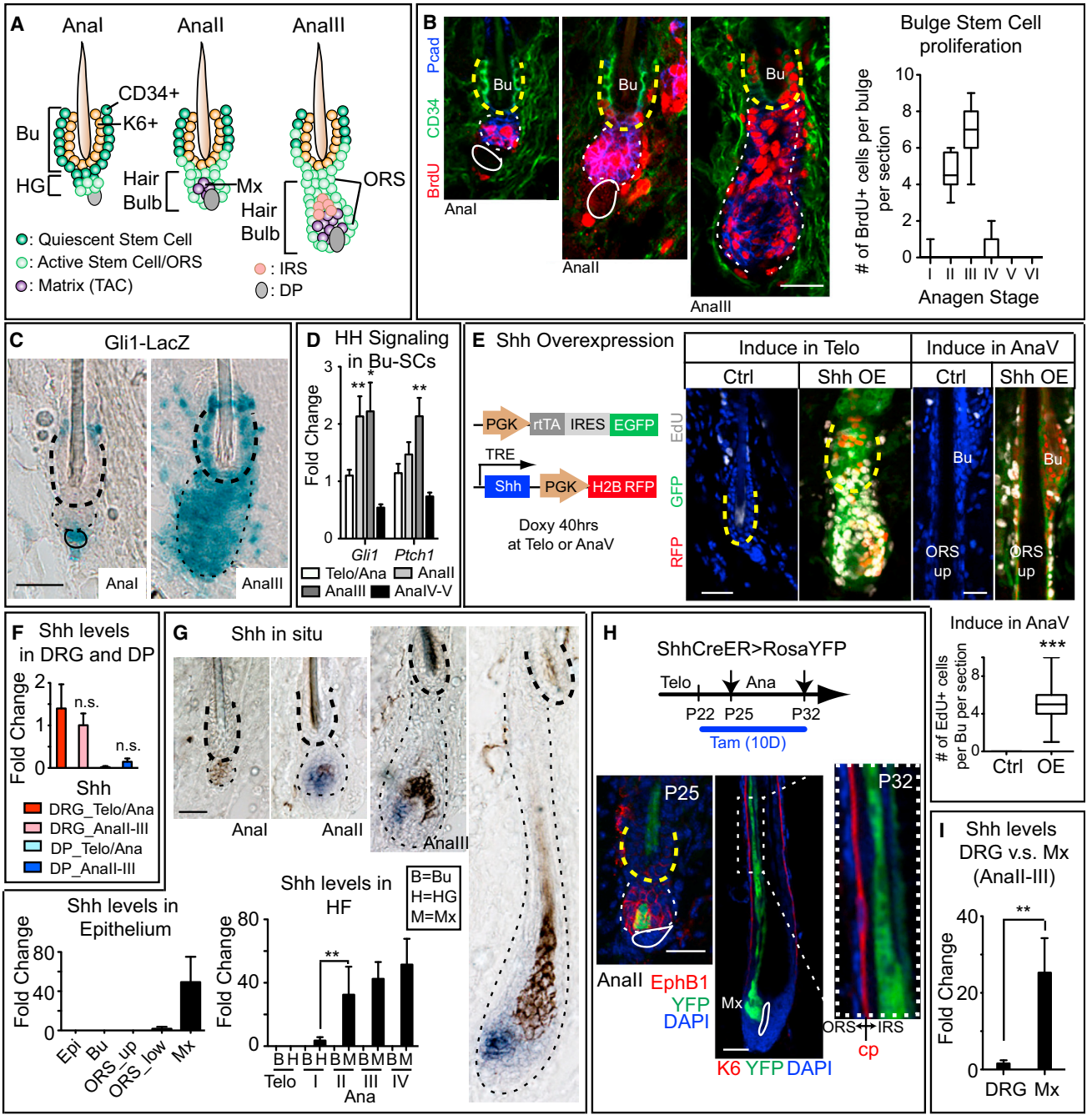

Figure 1. HH Pathway Activity in Bu-SCs Is Upregulated upon Bu-SC Activation Concurrent with Matrix SHH Expression, whereas SHH Overexpression Induces Bu-SC Proliferation

(A) Schematics of early anagen from AnaI–III. The AnaII hair bulb contains newly emerged matrix (Mx). From AnaIII and onward, the HG structure is no longer obvious.

(B) Time course monitoring of BrdU$^+$ cells during anagen and quantifications. Bulge: CD34$^+$ (in green) and yellow dashed lines. HG/hair bulb: Pcad$^+$ (in blue) and white dashed lines. Solid lines, DP (≥30 HFs from 2–3 animals per substage).

(C) β-galactosidase activity (blue) of *Gli1-LacZ* HFs at AnaI and AnaIII. Bulge, thick dashed lines; hair bulb, thin dashed lines; solid lines, DP.

(D) RT-PCR of *Gli1* and *Ptch1* from purified Bu-SCs at different substages.

(E) Schematics and results of *Shh* overexpression in telogen and AnaV compared to controls.

(F) RT-PCR examining *Shh* expression in dissected DRGs and FACS-purified DP.

(G) In situ hybridization (purple) and RT-PCR examining *Shh* levels in different compartments within epithelium.

(legend continued on next page)

2014). Hair regeneration is fueled by hair follicle stem cells (HFSCs) in the bulge (Bu-SCs) and a small cluster of cells beneath it, known as the secondary hair germ (HG) (Morris et al., 2004; Rompolas et al., 2013). In turn, the HG directly abuts a mesenchymal structure, called the dermal papillae (DP) (Figure 1A).

Many tissues have two populations of SCs with distinctive proliferative characteristics: a more quiescent population that cycles infrequently (quiescent SCs) and a primed population that is more sensitive to activation (primed SCs) (Li and Clevers, 2010). In HFs, Bu-SCs and HG represent these two respective populations. Bu-SCs and HG share many molecular features. However, HG cells are always first to proliferate upon anagen entry and in vitro generate larger colonies more quickly than Bu-SCs (Greco et al., 2009).

Both Bu-SCs and HG are quiescent during telogen. At anagen onset, HG responds to cues from DP and becomes active. Lineage-tracing experiments suggest that these proliferation events within HG lead to generation of matrix, the HF's TAC population, which has a molecular signature very different from that of Bu-SCs/HGs (Greco et al., 2009; Hsu et al., 2011; Lien et al., 2011; Rompolas et al., 2013). Matrix proliferates rapidly and, after several divisions, progresses to differentiate to make the hair shaft and its inner root sheath (IRS). By contrast, Bu-SCs proliferate 1–2 days later than HG and are the major source for outer root sheath (ORS) cells that encase the newly regenerating HF as it grows downward and expands the distance between bulge and matrix (Hsu et al., 2011; Rompolas et al., 2013). At catagen, the matrix apoptoses, but some ORS cells are spared, forming a new bulge and a new HG to sustain the next hair cycle. The adjacent old bulge has no HG or DP and serves only as a SC reservoir for use upon injury and a means to anchor the hair generated in the previous cycle (Hsu et al., 2011).

Several niche components and factors influence hair cycle progression. During telogen, $K6^+$ bulge maintains Bu-SCs in a quiescent state, at least in part through BMP6 and FGF18 (Fantauzzo and Christiano, 2011; Hsu et al., 2011). The dermis also imposes macroenvironmental inhibitory cues, largely through BMP4 (Plikus et al., 2008). Overcoming this quiescence threshold to transition from telogen → anagen requires input from DP and adipocyte progenitors that also signal through DP, by transmitting activation cues such as BMP inhibitors, transforming growth factor β (TGF-β), platelet-derived growth factors (PDGFs), and fibroblast growth factor 7/10 (FGF7/10) (Festa et al., 2011; Greco et al., 2009; Oshimori and Fuchs, 2012). Together, these factors promote HG activation and anagen entry.

Although close proximity between DP and HG explains how HG is activated prior to Bu-SCs (Greco et al., 2009), it raises a question of how Bu-SCs become activated. When anagen begins, the DP is increasingly pushed downward as the matrix pool emerges and expands and the ORS forms. At the time of Bu-SC activation, DP is even further away from bulge than at anagen entry (Figure 1A). Hence, it seems unlikely that the same mechanism triggering HG activation is involved in Bu-SC activation. That said, neither a specific niche cell type nor Bu-SC proliferation-inducing signal has been identified to account for the behavior of these more quiescent SCs during tissue regeneration. In the present study, we explore this fascinating and important issue.

RESULTS

HG and Bulge Stem Cells Exhibit Different Signaling Responses upon Activation

Anagen is subdivided into six substages (AnaI–VI), based upon morphology and length of the regenerating HF (Müller-Röver et al., 2001). Morphologically, AnaI resembles telogen except for a slight expansion of HG, as these cells become proliferative. By AnaII, the growing HG starts to produce matrix (LEF1, P-cadherin double-positive) that envelops the DP. Between AnaII and AnaIII, HG structure is no longer obvious, and emerging HF has doubled in size, displacing DP and matrix by at least 100 μm from the bulge. Signs of IRS differentiation appear, and shortly thereafter, hair shaft begins to form (Figures 1A and S1A available online).

To pinpoint the anagen substage at which Bu-SCs proliferate, we conducted BrdU incorporation assays. Bu-SCs began to proliferate at AnaII and peaked by AnaIII; by AnaV, they had returned to quiescence (Figure 1B). This activation pattern and timing did not vary with genetic strain or sex (Figures S1B and S1C), implying that Bu-SC activation is selectively and discretely controlled at AnaII onset through AnaIII.

Since DP had already moved away from bulge by AnaII, we asked how Bu-SCs become activated. We first tested whether canonical WNT and TGF-β2 pathways are induced in activated Bu-SCs as they are in activated HG (Greco et al., 2009; Oshimori and Fuchs, 2012). RT-PCR analyses of Bu-SCs purified at different hair cycle substages showed that neither WNT target *Axin2* nor TGF-β2 target *Tmeff1* was appreciably elevated at AnaII–III (Figure S1D). We next examined known SC quiescence factors in the environs to see whether these might be downregulated. However, *Bmp6* and *Fgf18* in $K6^+$ bulge and *Bmp4* in dermis were maintained if not elevated at this transition, as was BMP target *Id1* in Bu-SCs (Figure S1E). These results suggested that in sharp contrast to HG, most Bu-SCs do not display elevated WNT or TGF-β responses, nor do they exhibit stronger signs of BMP inhibition upon activation.

We next searched for other pathways that might account for Bu-SC activation. Hedgehog (HH) agonists and/or ectopic dermal Sonic HH (SHH) can induce anagen (Paladini et al., 2005; Sato et al., 1999), and systemic delivery of pan-HH-blocking antibodies delay it (Wang et al., 2000), suggesting that the HH pathway might be involved. All three HHs have been reported to express in cells surrounding HFs: SHH is

(H) Tamoxifen-treated *Shh-CreER>RosaYFP* HFs at different anagen substages. EphrinB1 (EphB1) marks the hair bulb. Companion layer (Cp) is $K6^+$ and is sandwiched between IRS and ORS. YFP^+ cells are only seen in IRS not ORS.

(I) RT-PCR of *Shh* from DRG and FACS-purified matrix.

Data are mean ± SD. *$p < 0.05$; **$p < 0.01$; ***$p < 0.001$. n.s.: not significant. Box-and-whisker plots: midline, median; box, 25th and 75th percentiles; whiskers, minimum and maximum. Scale bars: 30 μm.

expressed by sensory neurons that innervate the region just above bulge (Brownell et al., 2011; Li et al., 2011), whereas Indian HH (IHH) and Desert HH (DHH) have been detected in DP (Driskell et al., 2009; Rendl et al., 2005).

Consistent with these reports, activity of HH reporter *Gli1-LacZ* was observed in DP and cells right above bulge at the telogen→AnaI transition (Figure 1C, left panel). Surprisingly, at AnaIII, *Gli1-LacZ* activity was markedly elevated throughout the entire bulge and hair bulb (right panel). Although LacZ activity remained strong in matrix-TACs, it quickly waned in bulge as anagen progressed (Figure S1G, upper panel). Analogously, RT-PCR showed that within Bu-SCs, expression of HH targets *Gli1* and *Ptch1* peaked specifically at AnaII–III (Figure 1D). These findings revealed that the two-step mechanism for SC activation entails not only spatial and temporal differences in activating Bu-SCs versus HG (Greco et al., 2009) but also distinct responses to different activation signals.

Overexpression of SHH Results in Aberrant Bu-SC Activation

We next asked whether altering HH pathway activity would perturb timing of Bu-SC activation. For this, we induced ectopic *Shh* expression in adult skin by cotransducing embryonic day (E) 9.5 epidermis in utero with one lentivirus constitutively expressing tetracycline-inducible transactivator *rtTA* coupled bicistronically to *EGFP* and another harboring an H2BRFP transgene and an *Shh* gene controlled by an rtTA response element (Chang et al., 2013). When *Shh* was induced in telogen, precocious anagen was triggered within 40 hr in all cotransduced HFs, whereas control littermates remained in telogen. More importantly, if *Shh* was induced at AnaV, when control bulge and upper ORS SCs have returned to quiescence (Hsu et al., 2011), cotransduced HFs sustained SC proliferation and upregulation of *Gli1-LacZ* (Figures 1E and S1G). Together, these data suggested that quiescent SCs proliferate in response to elevated SHH.

Bulge Stem Cell Activation Coincides with the Appearance of Transit-Amplifying Progeny that Robustly Express SHH

To gain insights into which HH source(s) might be physiologically relevant for Bu-SC activation, we first determined whether Bu-SCs and cells within the environs alter their *Hh* expression specifically at AnaII–III (Figures 1F, 1G, and S1F). In contrast to prior claims (Xiong et al., 2013), Bu-SCs do not express *Shh* (Lien et al., 2011) (Figure 1G). Moreover, from AnaI→III, none of the three *Hhs* were upregulated in DP or dorsal root ganglia (DRG, harboring cutaneous neuronal cell bodies) (Figure 1F). RT-PCR and in situ hybridizations further revealed that *Shh* was also low/absent in epidermis and in ORS (Figure 1G). Similarly, it was barely detectable in HGs of telogen or AnaI HFs. By AnaII, however, *Shh* was robustly upregulated in HFs, concomitant with matrix specification. Thereafter, *Shh* expression remained high and restricted to matrix-TACs until their degeneration during catagen (Figure 1G).

Lineage tracing further demonstrated that *Shh*$^+$ cells in AnaII HFs are matrix precursors, given that when *Shh*-CreER (Harfe et al., 2004) was activated at telogen and sustained through anagen for 10 days, Rosa26-YFP$^+$ cells first appeared in a subset of AnaII hair bulb cells and later in matrix and IRS of full-anagen HFs (Figure 1H). Epidermis, bulge, and entire ORS remained YFP$^-$ even under sustained CreER induction. We further confirmed by in situ hybridization that IRS cells do not express *Shh*. Their YFP marks are due to their YFP$^+$ matrix origin: Thus, when *Shh-CreER* was induced in full anagen and HFs were examined 48 hr later but preceding IRS generation, YFP was restricted to matrix-TACs. Notably, SHH levels in matrix were significantly higher than in cutaneous neurons, as revealed by *Shh*-CreER activity and RT-PCR (Figures 1I and S1H).

These data established that (1) epithelial SHH initiates specifically at AnaII in emerging matrix precursors and is sustained in matrix thereafter; (2) Bu-SC proliferation coincides with and is limited to AnaII–III, when matrix is still in relatively close proximity to bulge (less than 200 μm); and (3) HH levels in surrounding cell types remain constant and relatively low throughout anagen (I–VI).

TAC-Derived SHH Is Essential for Bulge Stem Cell Activation

To determine whether SHH produced by downstream TAC progeny is a critical factor in governing SC behavior, we engineered *K15-CrePGR; Shh^{null}/fl* mice and treated them with RU486 to knock out *Shh* in Bu-SCs and HG just prior to the 1st adult anagen entry (referred to as *Shh*-cKO). Since *Shh* is not expressed by either Bu-SCs or HG, this strategy leads to specific perturbation of SHH in the emerging matrix formed from HG (Figures S2A and S2B), without interfering with SHH from other sources. The dramatic differences in signaling responsiveness underscored the importance of comparing the same anagen substage when investigating SC activity. We did this for all analyses presented herein. In addition, because the 1st adult hair cycle in mouse backskin is synchronized, we performed analysis on this cycle unless specified.

HGs were still activated in Anal *Shh*-cKO HFs, suggesting that SHH is dispensable for this step. However, starting from AnaII, *Shh*-cKO HFs displayed significantly reduced proliferation not only in hair bulb and TACs, but also in Bu-SCs (Figure 2A). HFSC marker expression and apoptotic events were comparable to controls (Figure S2C and data not shown).

To test whether there is a role for neuronal-derived SHH in governing Bu-SC activation, we surgically ablated dorsal cutaneous nerves just prior to anagen onset. By AnaII (5 days after surgery), sensory nerves encasing HFs had degenerated, but Bu-SC proliferation was no different from the sham-operated control side (Figures 2B and S2D). Thus, Bu-SC activation relies upon SHH from TACs and not cutaneous sensory nerves.

Previously we showed that signals from the K6$^+$ bulge inhibit HFSC proliferation (Hsu et al., 2011). To assess relative contributions of K6$^+$ bulge and matrix-TACs to Bu-SC activation, we exploited hair plucking, which removes the K6$^+$ bulge. Interestingly, despite their more distant proximity, HG cells responded to this loss by proliferating within 24 hr and at least a full day prior to Bu-SCs (Figure 2C). This result revealed that (1) in the unperturbed niche, inhibitory cues secreted by the K6$^+$ bulge likely reach and influence HG; and (2) Bu-SC activation upon plucking may not simply arise from loss of inhibitory signals but might also require an activation cue. To address whether this cue is

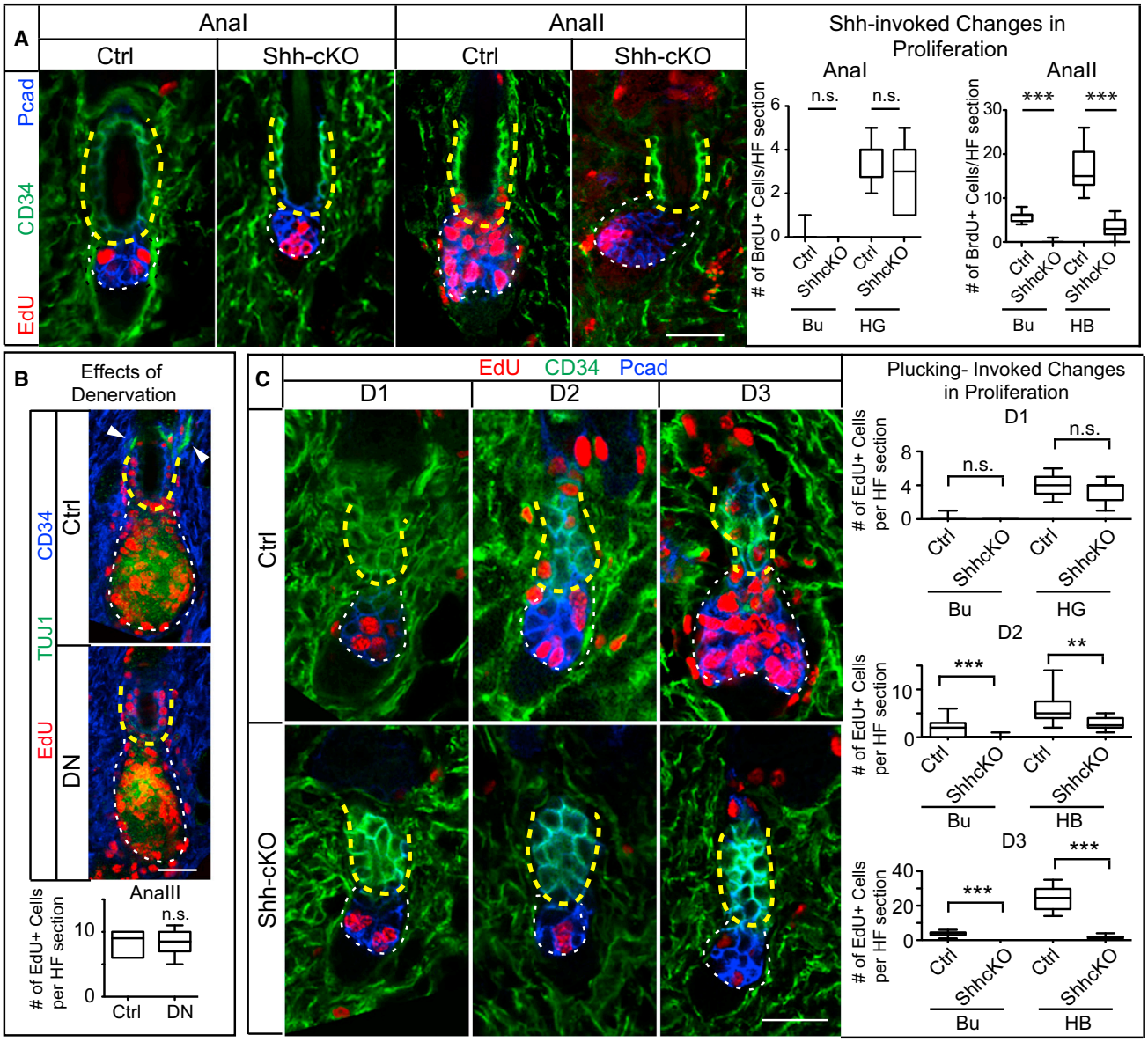

Figure 2. TAC-Derived SHH Is Essential for Bu-SC and Hair Bulb Proliferation during Normal and Plucking-Induced Hair Regeneration

(A) Conditional deletion of *Shh* from HFs impairs proliferation of both Bu-SCs and hair bulbs (n ≥ 2 mice, ≥ 12 HFs per mouse).

(B) Immunolocalization of EdU, CD34, and TUJ1 (pan-neuronal marker that also marks IRS) in AnaII HFs and quantifications of EdU^+ cells per bulge in sections from control and denervated side (DN) of same animal (n = 3 mice; ≥ 14 HFs per mice). Arrowheads: nerve fibers innervating the HF.

(C) HFs from WT and *Shh*-cKO were plucked during telogen at day (D) 0, and the proliferative statuses of Bu-SCs and hair bulbs were examined at D1, D2, and D3 post-plucking (n ≥ 2 mice, ≥ 8 HFs per mice).

Box-and-whisker plots are as in Figure 1 legend. **p < 0.01; ***p < 0.001. Bulge (Bu), yellow dashed lines; HG or hair bulb (HB), white dashed lines. Scale bars, 30 μm. n.s., not significant.

TAC-derived SHH, we repeated plucking experiments in *Shh*-cKO mice. During the first 24 hr, plucked *Shh*-cKO and control HFs both had robust EdU incorporation in HG. However and in striking contrast to control, *Shh*-cKO Bu-SCs remained quiescent (Figure 2C). In situ hybridization confirmed that in plucked control HFs, *Shh* is induced starting at 24 hr post-plucking, when the HG enlarges and TACs first appear. *Gli1* activation in Bu-SCs also showed a 24 hr delay after plucking (Figures S2E and S2F). Collectively, these data suggested that TAC-derived SHH is essential to trigger Bu-SC proliferation even when inhibitory cues are removed.

Activation of Bulge Stem Cells but Not HG Requires *Shh* Pathway Activity in the HF

We next wondered whether TAC-derived SHH exerts its effects by activating Bu-SCs directly. We first determined

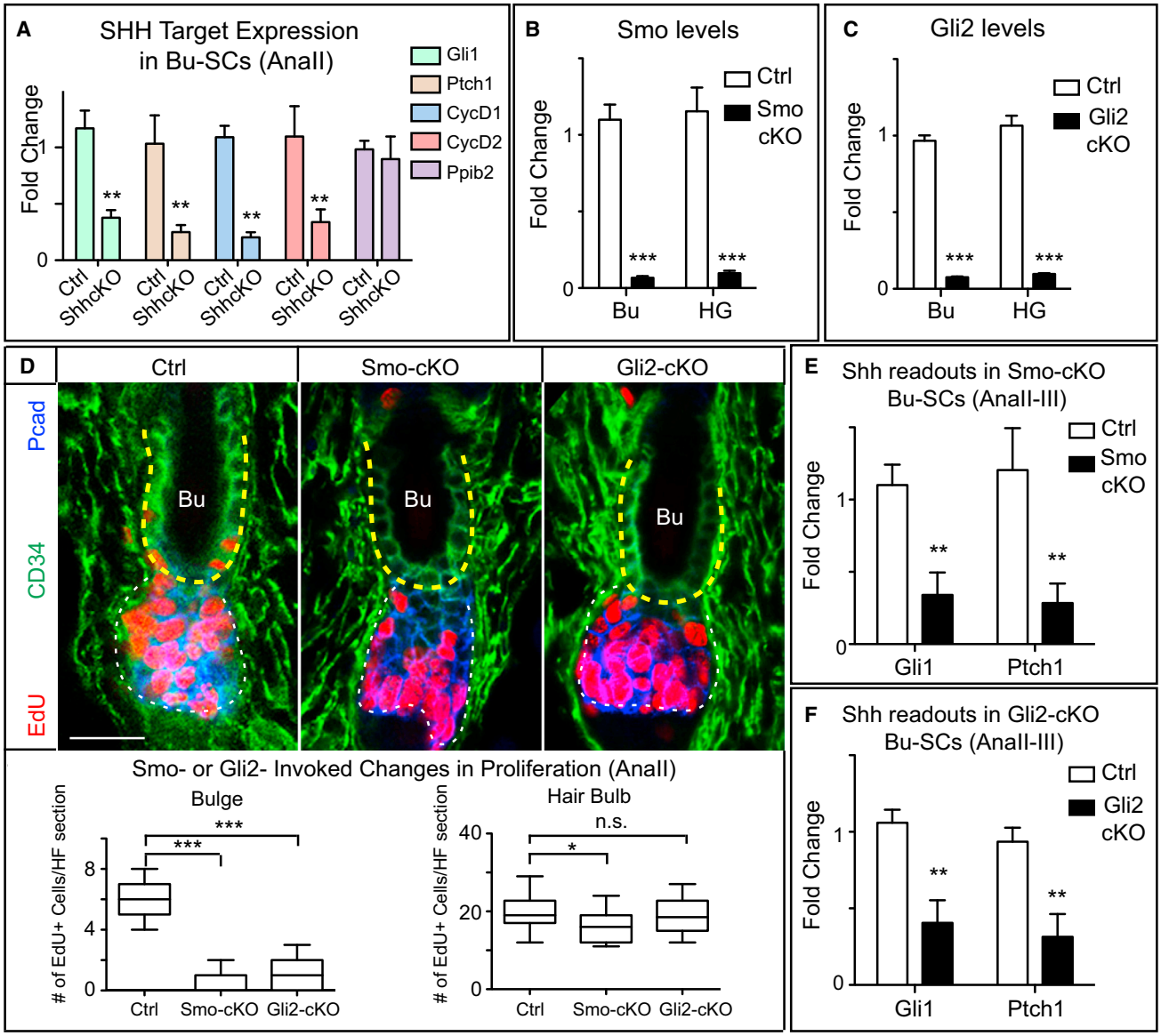

Figure 3. SHH Pathway Activity in the HF Is Critical for Bu-SC Activation

(A) RT-PCR of SHH targets in FACS-purified control or *Shh*-cKO Bu-SCs at AnaII. Known SHH targets are downregulated, and control gene Ppib2 is unchanged in *Shh*-cKO Bu-SCs.

(B) RT-PCR of *Smo* in FACS-purified Bu-SCs and HG in control and *Smo*-cKO.

(C) RT-PCR of *Gli2* in FACS-purified Bu-SCs and HG in control and *Gli2*-cKO.

(D) AnaII HFs from control, *Smo*-cKO, and *Gli2*-cKO, with immunolabeling of EdU, CD34, and Pcad. (n ≥ 3 per genotype, ≥ 14 HFs per mouse). Bulge, yellow dashed lines; hair bulb, white dashed lines. Box-and-whisker plots are as in Figure 1 legend. Scale bar, 30 μm.

(E and F) RT-PCR of *Gli1* and *Ptch1* in FACS-purified control, *Smo*-cKO, or *Gli2*-cKO Bu-SCs at AnaII–III.

Data are mean ± SD. n.s., not significant. *p < 0.05; **p < 0.01; ***p < 0.001.

whether endogenous SHH target genes are altered in Bu-SCs when SHH is not produced by matrix-TACs. In situ hybridizations showed that *Gli1* was downregulated in *Shh*-cKO HFs. RT-PCR analysis of purified AnaII *Shh*-cKO Bu-SCs further revealed that known SHH targets *Gli1*, *Patched-1* (*Ptch1*), *Cyclin D1* (*CycD1*), and *Cyclin D2* (*CycD2*) were all downregulated, reflective of a loss of SHH signaling within Bu-SCs (Figures 3A and S3A).

Upon SHH binding to its receptor PTCH1, Smoothened (SMO) is derepressed, and GLI transcription factors become activated (Beachy et al., 2010). We therefore asked whether removal of SHH downstream components from HFs would affect Bu-SC proliferation. Due to its high targeting efficiency, we used *Sox9-CreER* (Soeda et al., 2010) rather than *K15-CrePGR* to induce deletion of *Smo* and *Gli2* in telogen HG and Bu-SCs (Figures 3B and 3C).

Similar to *Shh*-cKO HFs, loss of *Smo* or *Gli2* had no major effect on HG activation. Rather, their deficiency resulted in a significant reduction in Bu-SC proliferation at AnaII (Figure 3D). *Gli1* and *Ptch1* expression were downregulated in *Smo*-cKO and *Gli2*-cKO Bu-SCs, as expected from their defective SHH signaling (Figures 3E and 3F). *Axin2* and *Tmeff1* expression was maintained, suggesting that WNT and TGF-β signaling operate normally in Bu-SCs deficient for SHH signaling (Figure S3B). Together, these data favor a requirement for SHH pathway activity in Bu-SC activation.

TACs Also Act on Heterologous Cell Types to Reinforce Other Niche Signaling Pathways

In contrast to the marked proliferative defects in AnaII *Shh*-cKO hair bulbs, proliferation was largely normal in hair bulbs lacking *Smo* or *Gli2* (Figures 2A and 3D). This difference could not be explained by gene-targeting efficiencies, which were uniformly high. Rather, it raised the possibility that in secreting SHH, emerging TACs may also influence other niche components, which then transmit additional key factors to maintain TAC proliferation.

To gain insights into possible cell type(s) and factors that might mediate such crosstalk, we first examined consequences of depleting TAC *Shh* on the expression of *Gli1* and *Ptch1* by various dermal cell types, including fibroblasts, adipocyte precursors, endothelial cells, and DP. DP showed the most dramatic and significant downregulation (Figures 4A, S3A, and S4A).

In early embryonic dermis, deficiency in HH signaling diminishes expression of BMP inhibitor NOGGIN (Woo et al., 2012). Interestingly, we found that in the adult, *Noggin* was upregulated in DP as HFs transitioned from Anal → AnaII–III; moreover, when *Shh* was ablated, this failed to occur (Figures 4B and 4C). DP-derived *Fgf7*, encoding another HG activation factor, behaved similarly to *Noggin* both in expression pattern and in response to loss of matrix-derived SHH. *Fgf10* and several other known dermal niche factors including *TGF-β2*, *Pdgfα*, and *Bmp4* were not altered in this way (Figures 4B and S4B).

By contrast, in SMO-deficient HFs, matrix-TACs still expressed *Shh,* and DP maintained normal levels of *Noggin*, *Fgf7*, and *Gli1* (Figures 4D, S4C, and S4D). This led us to surmise that matrix-derived SHH, still expressed in these mutants, promotes expression of these DP factors, thereby driving expansion of the SMO-deficient hair bulb. Indeed, NOGGIN and FGF7 each partially rescued hair bulb proliferation defects in *Shh*-cKO HFs (Figure 4E). Collectively, these findings showed that once TACs emerge, they secrete SHH to promote hair bulb expansion through DP-TAC crosstalk. When TACs cannot express SHH, this crosstalk is uncoupled, and DP in turn loses its potency to express factors needed to drive hair bulb proliferation.

Bulge Stem Cell Proliferation Relies Directly upon SHH Signaling Rather than Secondary Stimuli Induced by SHH Signaling

Given the secondary stimuli produced by SHH-activated DP, we sought to address whether Bu-SC proliferation relies directly upon SHH signaling or upon secondary stimuli generated by SHH. For this, we devised a strategy to perform mosaic inducible *Smo* knockdowns in vivo. If SHH signaling induces secondary stimuli that then drive Bu-SC proliferation, Bu-SCs should proliferate irrespective of whether they are SMO^{+} or SMO^{-}. If, however, Bu-SCs rely directly on SHH signaling to proliferate, SMO^{-} Bu-SCs will be compromised selectively.

To regulate mosaicism, we transduced E9.5 K14rtTA embryos with lentiviruses harboring inducible *Smo* or control (*luciferase*) shRNAs coupled with RFP (Figure 5A). As such, the potency of knockdown correlated positively with RFP levels and was confined to the epidermal lineage (Beronja et al., 2010; Dow et al., 2012). We first established that 8 days of induction was sufficient to achieve ~85% knockdown of *Smo* in RFP bright (RFP^{bri}) cells (Figures 5B, S5A, and S5B). When *Smo* knockdown was induced 8–10 days prior to AnaII, highly transduced HFs resembled *Smo*-cKO HFs, showing no Bu-SC proliferation. When transduced at lower titer so that >95% of HFs were mosaically infected and <10% Bu-SCs were RFP^{bri}, only *Smo* knockdown Bu-SCs (RFP^{bri}) displayed proliferation deficits and reduced *Gli1* and *Ptch1* expression (Figures 5C and 5D). Together, these data supported an autonomous requirement of SHH signaling for Bu-SC activation and unequivocally demonstrated that TACs directly control the proliferation of Bu-SCs through SHH (Figure S5C).

Gas1 Facilitates SHH Reception in Bulge Stem Cells

The dependency of Bu-SCs on SHH signaling was intriguing given that the distance between SHH-transmitting matrix-TACs and bulge reaches ~200 μm by the end of AnaIII. To understand how Bu-SCs maintain this long-range sensitivity, we were drawn to GAS1 (growth arrest-specific 1), a GPI-linked membrane coreceptor of PTCH1 that enhances SHH signaling (Allen et al., 2007; Martinelli and Fan, 2007). Microarray data showed that *Gas1* mRNA was enriched in Bu-SCs (Blanpain et al., 2004; Greco et al., 2009; Tumbar et al., 2004). Moreover, chromatin immunoprecipitation and Solexa sequencing (ChIP-seq) indicated that *Gas1* is actively transcribed in Bu-SCs but repressed in matrix-TACs (Lien et al., 2011) (Figure S6A). RT-PCR and immunofluorescence confirmed these findings and further showed that GAS1 is highly expressed not only in Bu-SCs but also in upper ORS, i.e., the future bulge (Figures 6A and S6B).

Similar to *Smo*- or *Gli2*-cKOs, *Gas1* mutants ($Gas1^{-/-}$) displayed significantly reduced proliferation in Bu-SCs but not hair bulb (Figures 6B and 6C). Because GAS1 was also present in dermis, we performed epithelial rescue experiments by transducing *K14rtTA+; $Gas1^{-/-}$* embryos with a Doxy-regulatable *Gas1* cDNA (Figure 6D) to assess whether GAS1 is required in the epithelium. When epithelial *Gas1* expression was restored at AnaIII, proliferation defects in $Gas1^{-/-}$ Bu-SCs were rescued, as was their reduced *Gli1* and *Ptch1* expression (Figures 6C–6E and S6C). Together, these data demonstrated that GAS1 enhances the ability of Bu-SCs to respond to SHH secreted by TACs.

Consequences of Defective Bulge Proliferation

The lack of HG and Bu-SC proliferation seen upon *Shh*-cKO ablation translated into a failure in HF down-growth and hair-coat recovery. When examined at 5, 18, and 25 days after AnaII, HFs still displayed AnaII morphology, suggesting that the hair

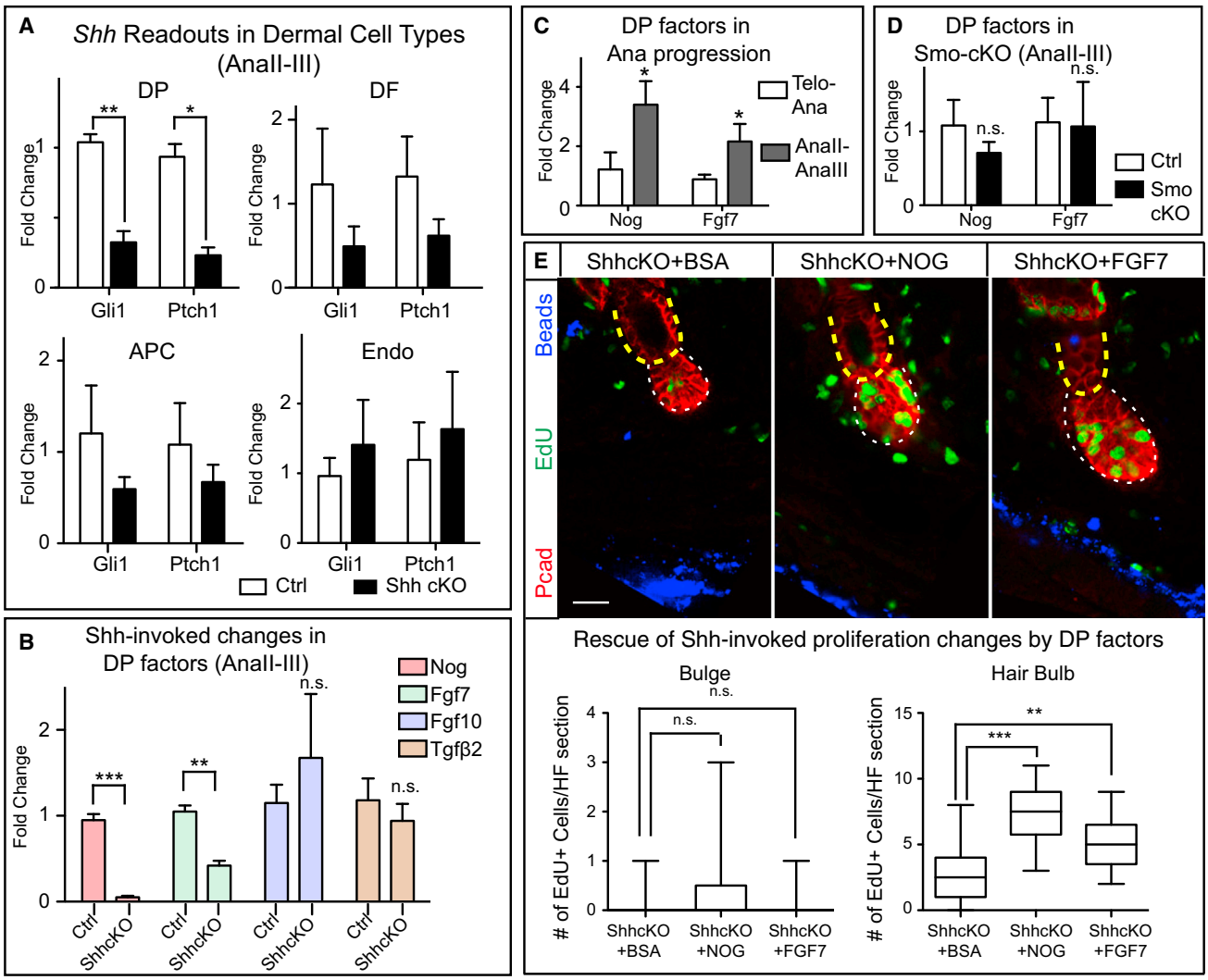

Figure 4. TAC-Derived SHH Maintains the Expression of DP Activation Signals

(A) RT-PCR of *Gli1* and *Ptch1* in FACS-purified DP, DF, adipocyte precursor cells (APC), and endothelial cells (Endo) from control and *Shh*-cKO at AnaII–III.

(B) RT-PCR of DP factors in FACS-purified control and *Shh*-cKO DP at AnaII–III.

(C) RT-PCR of *Nog* and *Fgf7* at telogen→anagen transition and at AnaII–III.

(D) RT-PCR of *Nog* and *Fgf7* in control and *Smo*-cKO DP at AnaII–III.

(E) BSA, NOGGIN, or FGF7 was coinjected with Cy5 fluorescent beads (blue) into *Shh*-cKO skin for 3 days, followed by EdU administration at D3 and analysis at D4 (n = 3 mice per experiment; ≥ 12 HFs per mouse). Bulge, yellow dashed lines; hair bulb, white dashed lines.

Box-and-whisker plots are as in Figure 1 legend. Scale bars, 30 μm. Data are mean ± SD. n.s., not significant. *p < 0.05; **p < 0.01; ***p < 0.001.

cycle was arrested (Figure S7A and data not shown). The effects on HF regeneration were less severe in *Smo*-cKO, as expected by the largely uncompromised SHH signaling in DP. However, *Smo*-cKO HFs were nevertheless shorter than normal and displayed proliferation defects in mature matrix and ORS, which led to a deficit in hair-coat recovery (Figure S7A). Thus, even though AnaII hair bulb proliferation was stimulated mainly by DP factors and unperturbed by SMO loss, matrix proliferation in full anagen required SHH signaling in the HF.

In contrast to *Shh*-cKO or *Smo*-cKO, *Gli2*-cKO HFs progressed through anagen despite a severe defect in Bu-SC proliferation and displayed normal ORS and matrix proliferation and a normal hair coat, without abnormal apoptosis (Figure S7A; data not shown). Similarly, even though the majority of *Gas1*$^{-/-}$ mice died before postnatal day (P) 30, HFs from rare surviving mice reached full anagen and displayed normal proliferation in ORS and matrix. These data indicate that for one cycle, Bu-SC proliferation is dispensable for anagen progression and hair regeneration.

To date, all mutations leading to altered HFSC activity affect either temporal activation of HG (Festa et al., 2011; Folgueras et al., 2013; Lowry et al., 2005; Oshimori and Fuchs, 2012) or proliferation of both Bu-SC and HG (Chen et al., 2012; Horsley et al., 2008; Kobielak et al., 2007). By targeting *Gli2,* we could

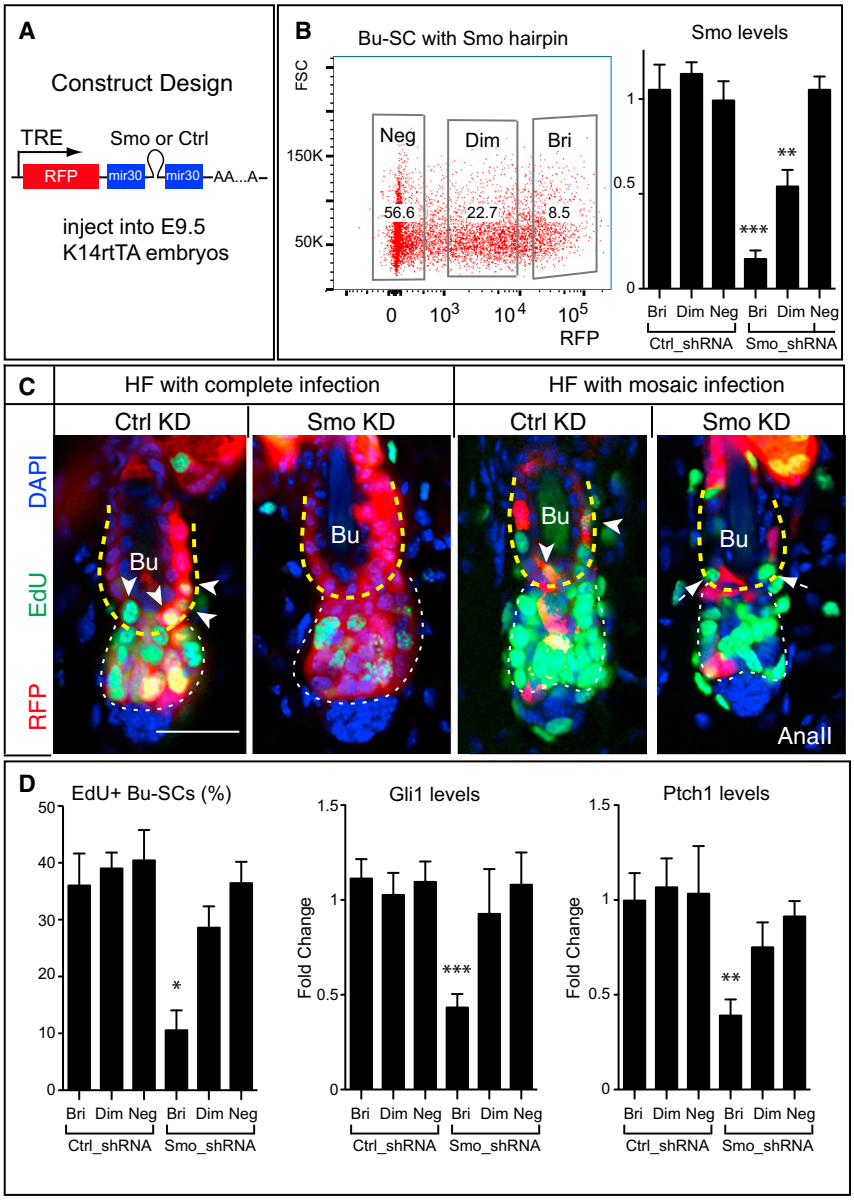

Figure 5. SHH Is Required Autonomously in Bu-SCs for Their Activation

(A) Lentiviral construct design.

(B) FACS plot of a mosaically transduced animal showing percentage of RFP^{bri} (Bri), RFP^{dim} (Dim), and RFP^{neg} (Neg) Bu-SCs and RT-PCR examining *Smo* from FACS-purified Bu-SCs infected with hairpins against *luciferase* (Ctrl_shRNA) or *Smo* (Smo_shRNA).

(C) AnaII HFs either completely infected or mosaically infected by Ctrl or *Smo* hairpins, immunolabeled with RFP and EdU. Arrowheads mark RFP and EdU double-positive Bu-SCs in HF infected with Ctrl_shRNA. Arrows mark EdU single-positive Bu-SCs in HF infected with Smo_shRNA.

(D) Quantifications of EdU incorporation and RT-PCR of *Gli1* and *Ptch1* in Ctrl- or *Smo*-shRNA-infected Bu-SCs (n = 2 per hairpins).

Bulge, yellow dashed lines; hair bulb, white dashed lines. Data are mean ± SD. Scale bars, 30 μm. *p < 0.05; **p < 0.01; ***p < 0.001.

selectively block Bu-SC proliferation without affecting proliferation in other populations, presenting a unique opportunity to assess whether Bu-SC proliferation has any contributions.

We first turned toward a possible defect in ORS, derived mainly from Bu-SCs (Hsu et al., 2011; Rompolas et al., 2013). Indeed, full-anagen *Gli2*-cKO HFs are shorter, indicating that their ORS is shorter (Figure S7A). Because new bulge and HG of telogen HFs are derived from ORS of the previous anagen (Hsu et al., 2011), we then followed these *Gli2*-cKO HFs into 2nd telogen. The new bulge of *Gli2*-cKO HFs was of normal size, but HG cell numbers were significantly reduced compared to controls (Figure 7A). Moreover, when *Gli2* was depleted efficiently after Bu-SCs returned to quiescence (1st AnaIV), or in the 2nd telogen prior to hair cycling, HG size in *Gli2*-cKO HFs was indistinguishable from that in controls (Figure S7B). Thus, although a nonproliferative function of *Gli2* cannot be formally excluded, these results favored the view that the defect in HG cell reduction is mainly due to a requirement for GLI2 in Bu-SC proliferation, without which ORS cannot be fully fueled, compromising HG size for the next cycle.

To test whether the new bulge and HG derived from defective Bu-SC proliferation in *Gli2*-cKO HFs are functionally equivalent to their wild-type (WT) counterparts, we knocked out *Gli2* in 1st telogen, allowed mice to complete one cycle, and then subjected 2nd telogen *Gli2*-cKO and control HFs to hair depilation and regeneration assays. With one round of depilation, initial matrix formation was delayed in *Gli2*-cKO HFs, Bu-SC proliferation was defective, and HF regeneration lagged behind controls. To determine which of these defects were attributable to fewer HG cells formed in *Gli2*-cKO HFs, we knocked out *Gli2* in 2nd telogen just prior to hair depilation, i.e., when HFs lacked *Gli2* but had a normal HG ($Gli2\text{-cKO}^{KO2telo}$). These $Gli2\text{-cKO}^{KO2telo}$ HFs were still defective in Bu-SC proliferation and had shortened ORS length, but matrix formation and regeneration speed were comparable to controls (Figures 7B and S7C and data not shown). Together, these data indicated that smaller HG size delays anagen progression. More importantly, the findings revealed that quiescent SCs (Bu-SCs) and primed SCs (HG) influence each other's production in an unforeseen way: primed SCs regulate quiescent-SC proliferation by generating its activation center TACs, and in turn, activation of quiescent SCs governs the formation of primed SC formation at the end of the cycle.

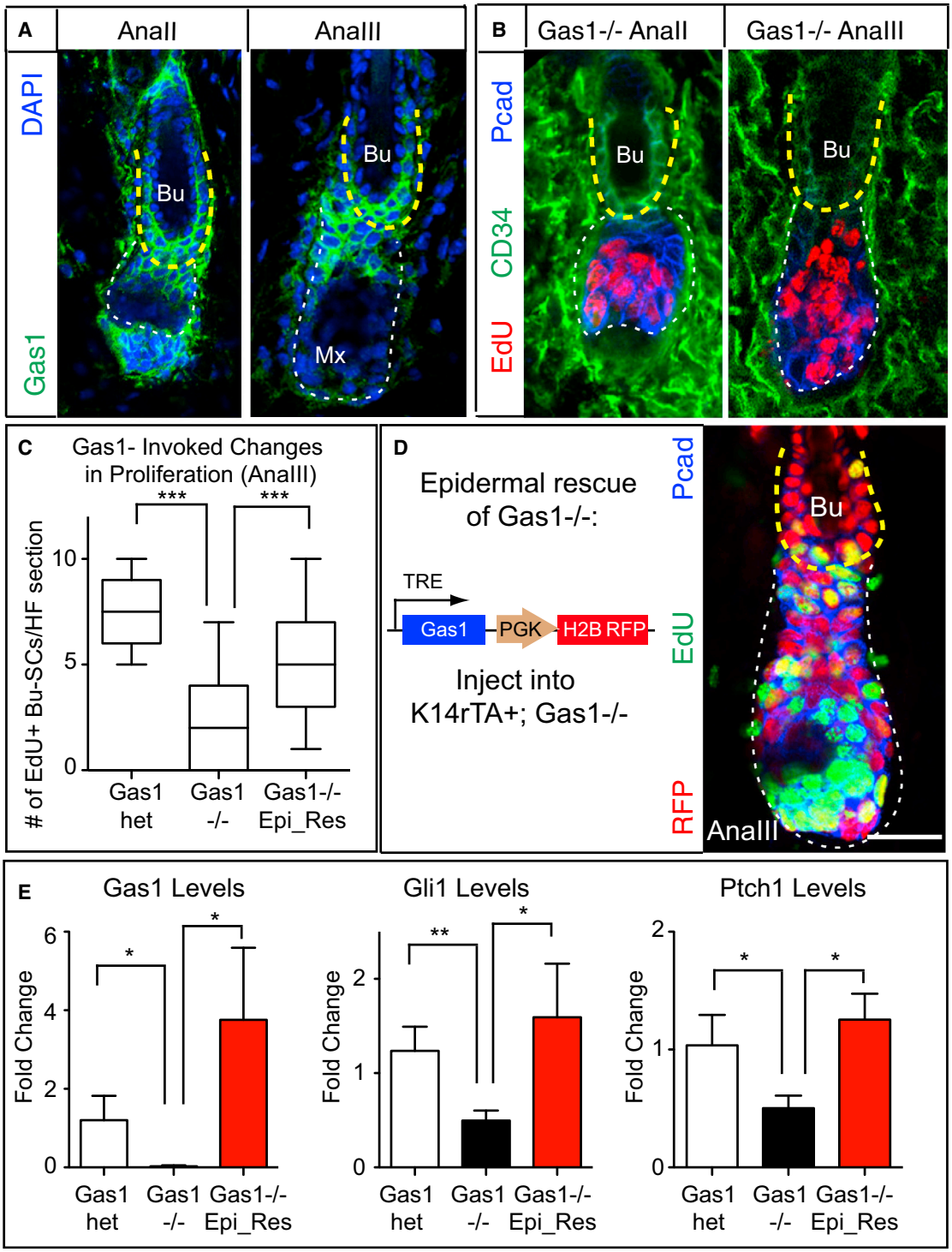

Figure 6. GAS1 Is Important for Proper Bu-SC Activation

(A) Immunodetection of GAS1.

(B) *Gas1*$^{-/-}$ HFs immunolabeled with EdU, CD34, and Pcad.

(C) Quantifications of EdU incorporation in AnaIII Bu-SCs from *Gas1*^{het}, *Gas1*$^{-/-}$, and *Gas1*$^{-/-}$ with epidermal rescue of GAS1 expression (n ≥ 2 mice, ≥ 14 HFs per mouse).

(D) (Left) Experimental strategy and lentiviral construct design. GAS1 was turned on by feeding the infected mice with Doxy chow 3 days prior to anagen entry until the time of analysis. (Right) AnaIII *Gas1*$^{-/-}$ HF with GAS1 expression restored in the epidermal compartment. Tissue is immunolabeled for RFP, EdU, and P-cadherin.

(legend continued on next page)

With a dysfunctional HG and defective Bu-SC proliferation, additional deficits occurred in *Gli2*-cKO HFs following subsequent rounds of cycling: whether induced by depilation or by natural aging, each *Gli2*-cKO hair cycle resulted in a gradually smaller HG and dwindling of Bu-SC numbers (Figures 7C–7F). Some *Gli2*-cKO HFs failed to regenerate completely, yielding a sparser hair coat relative to controls (Figure S7D). These data established that without sufficient input from Bu-SCs, the formations of first a new HG and then Bu-SCs are affected. In addition, the functionality of remaining HFSCs is compromised, manifested by their inability to regenerate new HFs over time. Collectively, these data underscore the critical importance of Bu-SC proliferation in maintaining long-term regeneration capacity of the HF system.

DISCUSSION

Dissecting Complex Niche Circuitry Regulating Stem Cell Behavior

Each SC niche varies in complexity, cell types, and signaling circuitry, which has made their identification and characterization a challenging task, particularly in complex mammalian tissues. Identifying the neighboring cell type(s) surrounding SCs has yielded insights into putative niche compositions (Méndez-Ferrer et al., 2010), and interfering with niche components has revealed functional importance of some niche cell types (Hsu et al., 2011; Raaijmakers et al., 2010; Rompolas et al., 2012; Zhang et al., 2003). Establishing the importance of a specific signal originating from a particular cell type can be achieved in part by selectively deleting a signaling factor from a niche component (Ding and Morrison, 2013; Ding et al., 2012). However, despite their indisputable value, these strategies do not unearth whether a signal acts directly on SCs or on a different niche cell type, which might then relay secondary signals to SCs. Moreover, if signals are knocked out during embryogenesis and analyzed in adults, it is not easy to distinguish primary from cumulative effects. Here, we attempted to tackle these hurdles by targeting both a signal emanating from the niche and the signal's critical downstream components within SCs. With high precision, we unveiled both direct and indirect functions of a specific niche factor, SHH.

BRG1, a chromatin-remodeling enzyme, has been proposed to form a regulatory loop with SHH to activate each other's expression in HFs (Xiong et al., 2013). However, HFs lacking *Brg1* differ markedly from those lacking *Shh*: *Brg1* mutants produce full-anagen HFs, whereas *Shh*-cKO HFs arrest in AnaII. Thus, if *Shh* is ever lost in *Brg1* mutants, it must happen in mature anagen, when matrix has moved too far away to influence Bu-SCs. In addition, *Brg1* mutants rapidly lose their hairs during telogen, implying a defect in hair anchorage, not tissue regeneration. By contrast, although HFs cannot regenerate following *Shh* ablation, old club hairs formed from morphogenesis are maintained for months. *Brg1*-cKO HFs also display more severe abnormalities than *Smo*-cKO or *Gli2*-cKO HFs. Overall, *Brg1* phenotypes appear to be complex and likely independent of SHH.

Previous studies highlight the importance of SHH signaling in embryonic HF development (Chiang et al., 1999; Gritli-Linde et al., 2007; Jamora et al., 2003; Mill et al., 2003; St-Jacques et al., 1998). Some differences arise when comparing SHH's functions in hair morphogenesis and adult hair regeneration: First, although HH signaling induces *Noggin* in embryonic mesenchyme prior to DP maturation, and as it does in adult DP, this is dispensable for embryonic placode proliferation (Woo et al., 2012). Second, once DP forms, SHH can act on it to coordinate additional stimuli such as *Fgf7*. Third, while *Gli2* is essential for down-growth of embryonic hair placodes, in adult HFs, it is only required in Bu-SCs and may act redundantly with other *Gli* transcription factors in other compartments. These comparisons suggest that even though adult SCs have adapted similar pathways that are operative during their development, the functions and mechanisms of action of these pathways can be different, highlighting the importance of using inducible approaches to study adult SC niches.

The Transit-Amplifying Pool Is an Active Signaling Center that Orchestrates Tissue Regeneration

Traditionally, TACs have been viewed as passive intermediates in tissue production. Our study unearthed several new and unforeseen functions for TACs that go well beyond the mere generation of terminally differentiated cells. First, we discovered that emerging TACs communicate directly to quiescent SCs and promote their proliferation, a process that happens when TACs are less than 200 μm from the bulge. As the HF grows downward and the ORS elongates, the matrix-TAC pool progressively moves away from the bulge and upper ORS. This provides a convenient mechanism to halt proliferation, so that the upper ORS, the cellular source for new Bu-SC and HG, has gone through only limited rounds of division. By contrast, starting from their emergence, TACs maintain close contact to DP. The TAC-DP crosstalk further promotes TAC proliferation to maximize rapid tissue production.

Collectively, our findings illustrate how a heterologous niche component (DP) can initiate tissue regeneration by stimulating primed SCs to establish a TAC pool, and then how TACs in turn can act as a signaling center to sustain DP signaling needed to expand the TAC pool. Equally important is the dual ability of TACs to stimulate proliferation of quiescent SCs. In this way, TACs are able to govern and integrate the timing and frequency of proliferation within these three epithelial populations: primed SCs, quiescent SCs, and TACs, thereby exquisitely regulating different phases and lineages involved in the regenerative process.

Most if not all tissues must sense different steps of a regeneration program and respond accordingly. In the HF, TACs provide positive signals, whereas differentiated $K6^+$ bulge provides

(E) RT-PCR examining levels of *Gas1*, *Gli1*, and *Ptch1* in FACS-purified AnaII Bu-SCs from $Gas1^{het}$, $Gas1^{-/-}$, and $Gas1^{-/-}$ with epidermal rescue of GAS1 expression.

Bulge, yellow dashed lines; hair bulb, white dashed lines. Box-and-whisker plots are as in Figure 1 legend. Scale bars, 30 μm. Data are mean ± SD. n.s., not significant. *$p < 0.05$; **$p < 0.01$; ***$p < 0.001$.

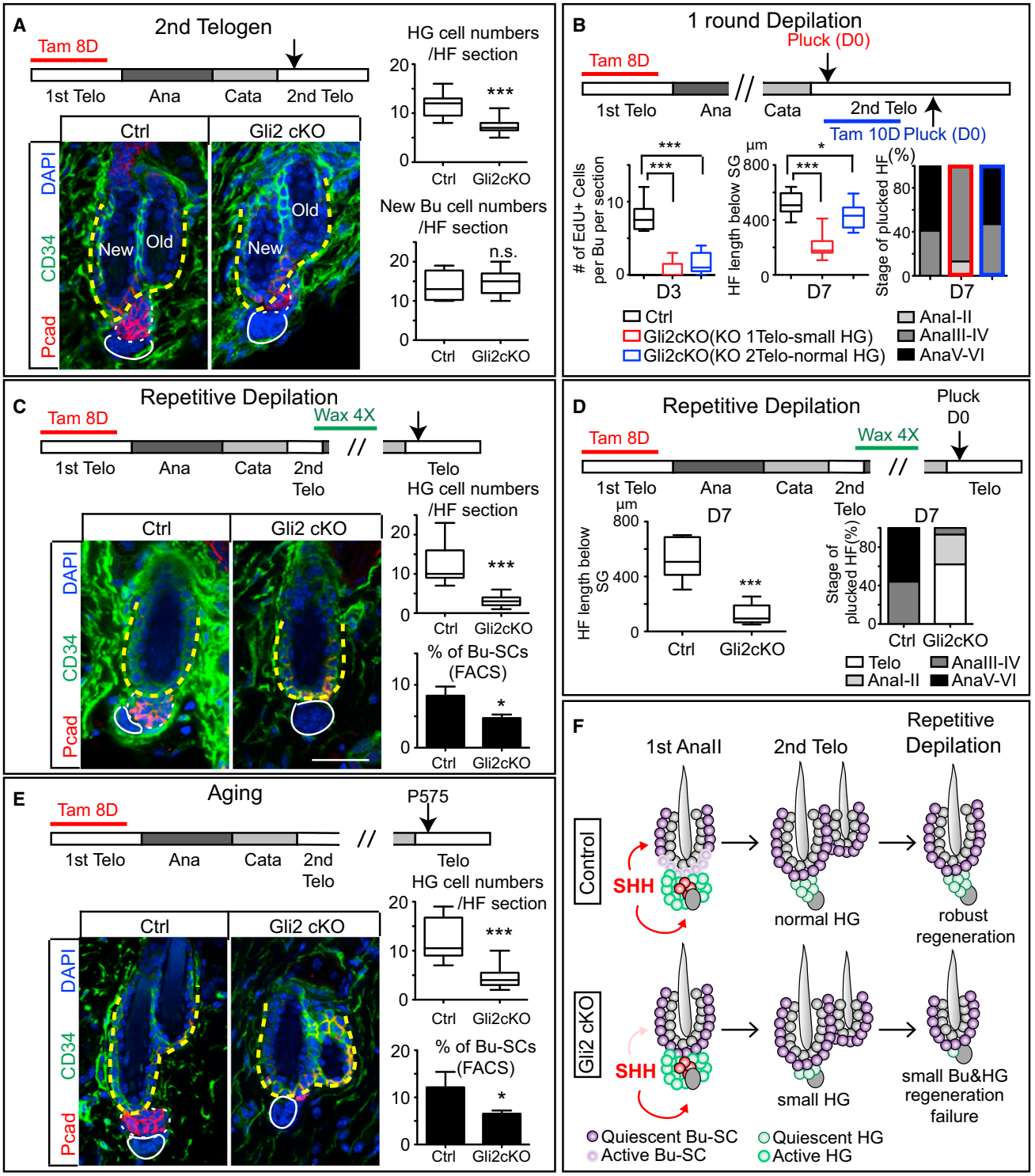

Figure 7. Defective Bu-SC Proliferation Leads to Reduced HG Cell Number Short-Term and Regeneration Failure Long-Term

(A) HG cell numbers are reduced after *Gli2*-cKO HFs complete one cycle. Examination was in 2nd telogen (n ≥ 3 mice, ≥ 18 HFs per mouse).

(B) Control and *Gli2*-cKO mice following one round of hair plucking. *Gli2* is knocked out in either 1st telogen (red bars) or 2nd telogen (blue bars). Plucking was performed in 2nd telogen. HFs were examined at D3 for Bu-SCs proliferation and at D7 for HF length (below sebaceous gland [SG]) and hair cycle stage (n ≥ 2 mice, ≥ 8 HFs per mouse).

(C) Control and *Gli2*-cKO HF after four waxings (n ≥ 3 mice, ≥ 21 HFs per mouse).

(legend continued on next page)

inhibitory signals to instruct SCs. By having two different progeny along the SC lineage to control tissue production, the SC→TAC→differentiated cell paradigm has a built-in mechanism to both fuel and gauge tissue production during its active phase and resume a quiescent state at its conclusion. By tailoring positive and negative signal providers to suit the particular needs of each tissue, these built-in feedback mechanisms can be an easy and effective way to ensure proper SC behavior during different phases of regeneration.

Extrinsic Mechanisms Regulate the Action of Quiescent versus Primed Stem Cell Populations

Many mammalian tissues, including the hematopoietic system, intestine, and HF, have both quiescent SCs and primed SCs (Buczacki et al., 2013; Fuchs, 2009; Greco et al., 2009; Li and Clevers, 2010; Wilson et al., 2008). Whether and how signals from the niche dictate the proliferative features of these two populations have remained poorly understood.

For the HF, insights into the governance of these two SC populations are now emerging. During telogen, inhibitory cues from both $K6^+$ bulge and dermal tissues impose a strong brake on both SC populations. Stimuli from DP eventually overpower inhibitory signals to activate primed SCs (HG), which respond first and make TACs. This essentially means that primed SCs must be activated and proliferate to a certain degree before the more quiescent ones can be activated. By invoking a dependency of Bu-SC proliferation on TACs and not DP, the more quiescent SCs become buffered from the occasional activation noise that might occur during the prolonged telogen phase. This ensures that influx from more quiescent SCs will not take place before TACs are generated and the regeneration process has been launched.

Coexistence of two SC populations also raises the question of whether contributions from both are essential for regeneration. In the HF, although reduction in primed-SC numbers or compromised primed-SC proliferation delays hair cycle progression right way, we showed here that the first cycle of regeneration takes place effectively without sufficient input from Bu-SCs. Therefore, the importance of Bu-SC proliferation is not to fuel immediate tissue production but rather to renew and maintain a functional pool of both primed and quiescent SCs over time. In this regard, it is intriguing that in male pattern baldness, quiescent SCs are largely normal, but primed-SC numbers shrink (Garza et al., 2011). Our study now provides functional insights for how this might arise and how this can affect hair regeneration short-term and long-term.

Lastly, although a common strategy to identify potential niche cells often involves searching for neighboring cell types immediately surrounding SCs, our results suggest that the effective range of specific niche signals may be a more important consideration than the distance between SC and specific niche cell types. They also raise a broader question as to whether SC niches should be defined on the basis of their proximity to SCs, their physiological role in SC governance, and whether their regulatory role is direct or indirect. As our knowledge of niche biology continues to expand, it seems reasonable to elaborate on earlier definitions and view the SC niche as a local ecosystem that maintains proper SC behavior though dynamic crosstalk and interactions between a diverse array of both heterologous cell types and SC progeny, which together ensure that tissue regeneration operates optimally and concomitantly with homeostatic and injury demands.

EXPERIMENTAL PROCEDURES

Mice

K6-RFP mice were generated by cloning a 7 kb fragment upstream of *Krt6a*. Other strains used and corresponding references are listed in the Extended Experimental Procedures. PGK-rTA or K14-rTA were activated by feeding mice with Doxy (2 mg/kg) chow with times specified. *Sox9-CreER* was activated by intraperitoneal (i.p.) injection (200 μg/g tamoxifen in corn oil) for 7–10 days in addition to topical application (20 mg/ml in ethanol) for 2 days. *K15-CrePGR* activation was by topical application of RU486 (4% in ethanol) for 8–10 days. BrdU (50 μg/g) or EdU (25 μg/g) was injected i.p. for two times within 24 hr before lethal administration of CO_2. Ultrasound-guided lentiviral injection procedures have been described (Beronja et al., 2010). All animals were maintained in an AAALAC-approved animal facility, and procedures were performed with IACUC-approved protocols.

Hair Cycle Timing

Subdivisions of hair cycle into six anagen stages were based on Müller-Röver et al. (2001). Since hair cycles vary among strains and sexes, stages instead of exact mouse ages were evaluated and carefully monitored for each experiment. Typically 3–5 mice of matched sex were analyzed. To enrich for populations from a specific anagen substage, the first hair cycle backskin was further divided into four quadrants: left-anterior, right-anterior, left-posterior, and right-posterior. The left quadrants were used for fluorescence-activated cell sorting (FACS), and the corresponding right quadrants were embedded in OCT for examination of hair cycle substages to ensure that > 80% of the HFs were in the exact substage indicated.

Statistical Analysis

Data were analyzed and statistics were performed using unpaired two-tailed Student's t test (Prism5 GraphPad). Significant differences between two groups were noted by asterisks (*$p < 0.05$; **$p < 0.01$: ***$p < 0.001$).

SUPPLEMENTAL INFORMATION

Supplemental Information includes Extended Experimental Procedures and seven figures and can be found with this article online at http://dx.doi.org/10.1016/j.cell.2014.02.057.

ACKNOWLEDGMENTS

We are grateful to C-M. Fan for $Gas1^{-/-}$, H. Westphal for the Shh^{null} mice, and many colleagues who donated mice to JAX; S. Mazel, L. Li, S. Semova, and S. Tadesse for sorting (RU FCRC facility, supported by NYSDOH Contract #C023046); RU Comparative Biology Center (AAALAC-accredited) for veterinary care; members of the Fuchs' lab, in particular, M. Kadaja for lentiviral constructs, C-Y. Chang, S-J. Luo, N. Oshimori, B. Keyes, and K. Tumaneng

(D) Control and *Gli2*-cKO HFs were plucked after four waxings and examined at D7 for HF length (below SG) and hair cycle stages (n ≥ 2 mice, ≥ 9 HF per mice).
(E) Aged control and *Gli2*-cKO HFs and quantifications.
(F) Model summarizing the results.
Bulge: $CD34^+$ (in green) and yellow dashed lines. HG: $Pcad^+$ (in red) and white dashed lines. Data are mean ± SD. *$p < 0.05$; ***$p < 0.001$. n.s., not significant. Box-and-whisker plots are as in Figure 1 legend. Scale bars, 30 μm.

for comments on the manuscript, L. Polak, N. Stokes, D. Oristian A. Aldeguer, and S. Hacker for assistance in mouse research, and J. Racelis for assistance with in situ hybridization. Y-C.H. was a NYSCF-Druckenmiller Postdoctoral Fellow and is now supported by NIH K99-R00 pathway to independence award K99-AR063127. L.L. is a Helen Hay Whitney Postdoctoral Fellow. E.F. is an HHMI Investigator. This work was supported by a grant (to E.F.) from the NIH/NIAMS (R01AR050452) and partially by a grant from Empire State Stem Cell (NYSTEM; N09G074), NYSTEM funds through NYSDOH (Contract C023046; RU FCRC).

Received: September 5, 2013
Revised: January 16, 2014
Accepted: February 24, 2014
Published: May 8, 2014

REFERENCES

Allen, B.L., Tenzen, T., and McMahon, A.P. (2007). The Hedgehog-binding proteins Gas1 and Cdo cooperate to positively regulate Shh signaling during mouse development. Genes Dev. *21*, 1244–1257.

Beachy, P.A., Hymowitz, S.G., Lazarus, R.A., Leahy, D.J., and Siebold, C. (2010). Interactions between Hedgehog proteins and their binding partners come into view. Genes Dev. *24*, 2001–2012.

Beronja, S., Livshits, G., Williams, S., and Fuchs, E. (2010). Rapid functional dissection of genetic networks via tissue-specific transduction and RNAi in mouse embryos. Nat. Med. *16*, 821–827.

Blanpain, C., Lowry, W.E., Geoghegan, A., Polak, L., and Fuchs, E. (2004). Self-renewal, multipotency, and the existence of two cell populations within an epithelial stem cell niche. Cell *118*, 635–648.

Brownell, I., Guevara, E., Bai, C.B., Loomis, C.A., and Joyner, A.L. (2011). Nerve-derived sonic hedgehog defines a niche for hair follicle stem cells capable of becoming epidermal stem cells. Cell Stem Cell *8*, 552–565.

Buczacki, S.J., Zecchini, H.I., Nicholson, A.M., Russell, R., Vermeulen, L., Kemp, R., and Winton, D.J. (2013). Intestinal label-retaining cells are secretory precursors expressing Lgr5. Nature *495*, 65–69.

Chang, C.Y., Pasolli, H.A., Giannopoulou, E.G., Guasch, G., Gronostajski, R.M., Elemento, O., and Fuchs, E. (2013). NFIB is a governor of epithelial-melanocyte stem cell behaviour in a shared niche. Nature *495*, 98–102.

Chen, T., Heller, E., Beronja, S., Oshimori, N., Stokes, N., and Fuchs, E. (2012). An RNA interference screen uncovers a new molecule in stem cell self-renewal and long-term regeneration. Nature *485*, 104–108.

Chiang, C., Swan, R.Z., Grachtchouk, M., Bolinger, M., Litingtung, Y., Robertson, E.K., Cooper, M.K., Gaffield, W., Westphal, H., Beachy, P.A., and Dlugosz, A.A. (1999). Essential role for Sonic hedgehog during hair follicle morphogenesis. Dev. Biol. *205*, 1–9.

Chow, A., Lucas, D., Hidalgo, A., Méndez-Ferrer, S., Hashimoto, D., Scheiermann, C., Battista, M., Leboeuf, M., Prophete, C., van Rooijen, N., et al. (2011). Bone marrow CD169+ macrophages promote the retention of hematopoietic stem and progenitor cells in the mesenchymal stem cell niche. J. Exp. Med. *208*, 261–271.

Ding, L., and Morrison, S.J. (2013). Haematopoietic stem cells and early lymphoid progenitors occupy distinct bone marrow niches. Nature *495*, 231–235.

Ding, L., Saunders, T.L., Enikolopov, G., and Morrison, S.J. (2012). Endothelial and perivascular cells maintain haematopoietic stem cells. Nature *481*, 457–462.

Dow, L.E., Premsrirut, P.K., Zuber, J., Fellmann, C., McJunkin, K., Miething, C., Park, Y., Dickins, R.A., Hannon, G.J., and Lowe, S.W. (2012). A pipeline for the generation of shRNA transgenic mice. Nat. Protoc. *7*, 374–393.

Driskell, R.R., Giangreco, A., Jensen, K.B., Mulder, K.W., and Watt, F.M. (2009). Sox2-positive dermal papilla cells specify hair follicle type in mammalian epidermis. Development *136*, 2815–2823.

Fantauzzo, K.A., and Christiano, A.M. (2011). There and back again: hair follicle stem cell dynamics. Cell Stem Cell *8*, 8–9.

Festa, E., Fretz, J., Berry, R., Schmidt, B., Rodeheffer, M., Horowitz, M., and Horsley, V. (2011). Adipocyte lineage cells contribute to the skin stem cell niche to drive hair cycling. Cell *146*, 761–771.

Folgueras, A.R., Guo, X., Pasolli, H.A., Stokes, N., Polak, L., Zheng, D., and Fuchs, E. (2013). Architectural niche organization by LHX2 is linked to hair follicle stem cell function. Cell Stem Cell *13*, 314–327.

Fuchs, E. (2009). The tortoise and the hair: slow-cycling cells in the stem cell race. Cell *137*, 811–819.

Garza, L.A., Yang, C.C., Zhao, T., Blatt, H.B., Lee, M., He, H., Stanton, D.C., Carrasco, L., Spiegel, J.H., Tobias, J.W., and Cotsarelis, G. (2011). Bald scalp in men with androgenetic alopecia retains hair follicle stem cells but lacks CD200-rich and CD34-positive hair follicle progenitor cells. J. Clin. Invest. *121*, 613–622.

Greco, V., Chen, T., Rendl, M., Schober, M., Pasolli, H.A., Stokes, N., Dela Cruz-Racelis, J., and Fuchs, E. (2009). A two-step mechanism for stem cell activation during hair regeneration. Cell Stem Cell *4*, 155–169.

Gritli-Linde, A., Hallberg, K., Harfe, B.D., Reyahi, A., Kannius-Janson, M., Nilsson, J., Cobourne, M.T., Sharpe, P.T., McMahon, A.P., and Linde, A. (2007). Abnormal hair development and apparent follicular transformation to mammary gland in the absence of hedgehog signaling. Dev. Cell *12*, 99–112.

Harfe, B.D., Scherz, P.J., Nissim, S., Tian, H., McMahon, A.P., and Tabin, C.J. (2004). Evidence for an expansion-based temporal Shh gradient in specifying vertebrate digit identities. Cell *118*, 517–528.

Horsley, V., Aliprantis, A.O., Polak, L., Glimcher, L.H., and Fuchs, E. (2008). NFATc1 balances quiescence and proliferation of skin stem cells. Cell *132*, 299–310.

Hsu, Y.C., and Fuchs, E. (2012). A family business: stem cell progeny join the niche to regulate homeostasis. Nat. Rev. Mol. Cell Biol. *13*, 103–114.

Hsu, Y.C., Pasolli, H.A., and Fuchs, E. (2011). Dynamics between stem cells, niche, and progeny in the hair follicle. Cell *144*, 92–105.

Jamora, C., DasGupta, R., Kocieniewski, P., and Fuchs, E. (2003). Links between signal transduction, transcription and adhesion in epithelial bud development. Nature *422*, 317–322.

Kobielak, K., Stokes, N., de la Cruz, J., Polak, L., and Fuchs, E. (2007). Loss of a quiescent niche but not follicle stem cells in the absence of bone morphogenetic protein signaling. Proc. Natl. Acad. Sci. USA *104*, 10063–10068.

Li, L., Rutlin, M., Abraira, V.E., Cassidy, C., Kus, L., Gong, S., Jankowski, M.P., Luo, W., Heintz, N., Koerber, H.R., et al. (2011). The functional organization of cutaneous low-threshold mechanosensory neurons. Cell *147*, 1615–1627.

Li, L.H., and Clevers, H. (2010). Coexistence of quiescent and active adult stem cells in mammals. Science *327*, 542–545.

Lien, W.H., Guo, X., Polak, L., Lawton, L.N., Young, R.A., Zheng, D., and Fuchs, E. (2011). Genome-wide maps of histone modifications unwind in vivo chromatin states of the hair follicle lineage. Cell Stem Cell *9*, 219–232.

Lowry, W.E., Blanpain, C., Nowak, J.A., Guasch, G., Lewis, L., and Fuchs, E. (2005). Defining the impact of beta-catenin/Tcf transactivation on epithelial stem cells. Genes Dev. *19*, 1596–1611.

Martinelli, D.C., and Fan, C.M. (2007). Gas1 extends the range of Hedgehog action by facilitating its signaling. Genes Dev. *21*, 1231–1243.

Méndez-Ferrer, S., Michurina, T.V., Ferraro, F., Mazloom, A.R., Macarthur, B.D., Lira, S.A., Scadden, D.T., Ma'ayan, A., Enikolopov, G.N., and Frenette, P.S. (2010). Mesenchymal and haematopoietic stem cells form a unique bone marrow niche. Nature *466*, 829–834.

Mill, P., Mo, R., Fu, H., Grachtchouk, M., Kim, P.C., Dlugosz, A.A., and Hui, C.C. (2003). Sonic hedgehog-dependent activation of Gli2 is essential for embryonic hair follicle development. Genes Dev. *17*, 282–294.

Mondal, B.C., Mukherjee, T., Mandal, L., Evans, C.J., Sinenko, S.A., Martinez-Agosto, J.A., and Banerjee, U. (2011). Interaction between differentiating cell- and niche-derived signals in hematopoietic progenitor maintenance. Cell *147*, 1589–1600.

Morris, R.J., Liu, Y., Marles, L., Yang, Z., Trempus, C., Li, S., Lin, J.S., Sawicki, J.A., and Cotsarelis, G. (2004). Capturing and profiling adult hair follicle stem cells. Nat. Biotechnol. *22*, 411–417.

Morrison, S.J., and Spradling, A.C. (2008). Stem cells and niches: mechanisms that promote stem cell maintenance throughout life. Cell *132*, 598–611.

Müller-Röver, S., Handjiski, B., van der Veen, C., Eichmüller, S., Foitzik, K., McKay, I.A., Stenn, K.S., and Paus, R. (2001). A comprehensive guide for the accurate classification of murine hair follicles in distinct hair cycle stages. J. Invest. Dermatol. *117*, 3–15.

Oshimori, N., and Fuchs, E. (2012). Paracrine TGF-β signaling counterbalances BMP-mediated repression in hair follicle stem cell activation. Cell Stem Cell *10*, 63–75.

Paladini, R.D., Saleh, J., Qian, C., Xu, G.X., and Rubin, L.L. (2005). Modulation of hair growth with small molecule agonists of the hedgehog signaling pathway. J. Invest. Dermatol. *125*, 638–646.

Pietras, E.M., Warr, M.R., and Passegué, E. (2011). Cell cycle regulation in hematopoietic stem cells. J. Cell Biol. *195*, 709–720.

Plikus, M.V., and Chuong, C.M. (2014). Macroenvironmental regulation of hair cycling and collective regenerative behavior. Cold Spring Harb. Perspect. Med. *4*, a015198.

Plikus, M.V., Mayer, J.A., de la Cruz, D., Baker, R.E., Maini, P.K., Maxson, R., and Chuong, C.M. (2008). Cyclic dermal BMP signalling regulates stem cell activation during hair regeneration. Nature *451*, 340–344.

Raaijmakers, M.H., Mukherjee, S., Guo, S., Zhang, S., Kobayashi, T., Schoonmaker, J.A., Ebert, B.L., Al-Shahrour, F., Hasserjian, R.P., Scadden, E.O., et al. (2010). Bone progenitor dysfunction induces myelodysplasia and secondary leukaemia. Nature *464*, 852–857.

Rendl, M., Lewis, L., and Fuchs, E. (2005). Molecular dissection of mesenchymal-epithelial interactions in the hair follicle. PLoS Biol. *3*, e331.

Rompolas, P., Deschene, E.R., Zito, G., Gonzalez, D.G., Saotome, I., Haberman, A.M., and Greco, V. (2012). Live imaging of stem cell and progeny behaviour in physiological hair-follicle regeneration. Nature *487*, 496–499.

Rompolas, P., Mesa, K.R., and Greco, V. (2013). Spatial organization within a niche as a determinant of stem-cell fate. Nature *502*, 513–518.

Sato, N., Leopold, P.L., and Crystal, R.G. (1999). Induction of the hair growth phase in postnatal mice by localized transient expression of Sonic hedgehog. J. Clin. Invest. *104*, 855–864.

Sato, T., van Es, J.H., Snippert, H.J., Stange, D.E., Vries, R.G., van den Born, M., Barker, N., Shroyer, N.F., van de Wetering, M., and Clevers, H. (2011). Paneth cells constitute the niche for Lgr5 stem cells in intestinal crypts. Nature *469*, 415–418.

Soeda, T., Deng, J.M., de Crombrugghe, B., Behringer, R.R., Nakamura, T., and Akiyama, H. (2010). Sox9-expressing precursors are the cellular origin of the cruciate ligament of the knee joint and the limb tendons. Genesis *48*, 635–644.

St-Jacques, B., Dassule, H.R., Karavanova, I., Botchkarev, V.A., Li, J., Danielian, P.S., McMahon, J.A., Lewis, P.M., Paus, R., and McMahon, A.P. (1998). Sonic hedgehog signaling is essential for hair development. Curr. Biol. *8*, 1058–1068.

Tumbar, T., Guasch, G., Greco, V., Blanpain, C., Lowry, W.E., Rendl, M., and Fuchs, E. (2004). Defining the epithelial stem cell niche in skin. Science *303*, 359–363.

Vied, C., Reilein, A., Field, N.S., and Kalderon, D. (2012). Regulation of stem cells by intersecting gradients of long-range niche signals. Dev. Cell *23*, 836–848.

Wang, L.C., Liu, Z.Y., Gambardella, L., Delacour, A., Shapiro, R., Yang, J., Sizing, I., Rayhorn, P., Garber, E.A., Benjamin, C.D., et al. (2000). Regular articles: conditional disruption of hedgehog signaling pathway defines its critical role in hair development and regeneration. J. Invest. Dermatol. *114*, 901–908.

Wilson, A., Laurenti, E., Oser, G., van der Wath, R.C., Blanco-Bose, W., Jaworski, M., Offner, S., Dunant, C.F., Eshkind, L., Bockamp, E., et al. (2008). Hematopoietic stem cells reversibly switch from dormancy to self-renewal during homeostasis and repair. Cell *135*, 1118–1129.

Winkler, I.G., Sims, N.A., Pettit, A.R., Barbier, V., Nowlan, B., Helwani, F., Poulton, I.J., van Rooijen, N., Alexander, K.A., Raggatt, L.J., and Lévesque, J.P. (2010). Bone marrow macrophages maintain hematopoietic stem cell (HSC) niches and their depletion mobilizes HSCs. Blood *116*, 4815–4828.

Woo, W.M., Zhen, H.H., and Oro, A.E. (2012). Shh maintains dermal papilla identity and hair morphogenesis via a Noggin-Shh regulatory loop. Genes Dev. *26*, 1235–1246.

Xiong, Y., Li, W., Shang, C., Chen, R.M., Han, P., Yang, J., Stankunas, K., Wu, B., Pan, M., Zhou, B., et al. (2013). Brg1 governs a positive feedback circuit in the hair follicle for tissue regeneration and repair. Dev. Cell *25*, 169–181.

Yilmaz, O.H., Valdez, R., Theisen, B.K., Guo, W., Ferguson, D.O., Wu, H., and Morrison, S.J. (2006). Pten dependence distinguishes haematopoietic stem cells from leukaemia-initiating cells. Nature *441*, 475–482.

Zhang, J.W., Niu, C., Ye, L., Huang, H.Y., He, X., Tong, W.G., Ross, J., Haug, J., Johnson, T., Feng, J.Q., et al. (2003). Identification of the haematopoietic stem cell niche and control of the niche size. Nature *425*, 836–841.

EXTENDED EXPERIMENTAL PROCEDURES

Mice

K14-rtTA, Shh-CreER, Sox9-CreER, K15-CrePGR, Smo^{flox}, Gli2^{flox}, Shh^{flox}, Shh^{neo}, Gas1^{Lacz}, Gli1^{Lacz}, and *Rosa26$^{Flox\text{-}Stop\text{-}Flox\text{-}YFP}$* (Bai et al., 2002; Chiang et al., 1999; Corrales et al., 2006; Dassule et al., 2000; Harfe et al., 2004; Long et al., 2001; Mao et al., 1999; Martinelli and Fan, 2007; Morris et al., 2004; Nguyen et al., 2006; Soeda et al., 2010; Srinivas et al., 2001) were described previously. *Lhx2-EGFP* mice were from The Gene Expression Nervous System Atlas (GENSAT) Project, NINDS Contracts N01NS02331 & HHSN271200723701C to The Rockefeller University (New York, NY, USA). *K6-RFP* mice were generated by cloning a 7 kb promoter sequence upstream of the mouse *Krt6a* gene and assembled with β-globin intron, mRFP, and poly(A) sequences. Transgenic mice were generated with standard pronuclear injections. To overexpress SHH in the hair follicle, the first 594 bp of mouse *Shh* is cloned after the Tet-responsive element (TRE) to produce an N terminus fragment of SHH same as the autocatalytic cleaved product. For intradermal injections of growth factors, recombinant NOGGIN (250 ng, R&D systems), FGF7 (250 ng, R&D systems), or BSA control was intradermally injected with FluoSpheres (Life Technologies).

Immunohistochemistry

The following antibodies and dilutions were used: CD34 (rat, 1:100, eBioscience), BrdU (rat, 1:100, Abcam), active-Caspases3 (rabbit, 1:500, R&D), GFP (rabbit, 1:500, Life Technologies or chicken, 1:2000, Abcam), P-cadherin (goat, 1:200, R&D or rat, 1:100, Fuchs lab), LEF1 (rabbit, 1:200 Fuchs Lab), AE15 (mouse, 1:300, Santa Cruz), CD140a (rat, 1:100, eBioscience), ALPL (goat, 1:200, R&D), CD31 (rat, 1:100, eBioscience), RFP (rabbit, 1:5000, MBL). Phospho-Histone H3 (rabbit, 1:500 Cell signaling). Nuclei were stained using 4'6'-diamidino-2-phenylindole (DAPI). EdU click-it reaction was performed according to manufacturer's directions (Life Technologies).

Histology and Immunofluorescence

For immunofluorescence microscopy of sagittal sections, backskins were embedded in OCT, frozen, cryosectioned (14–30 μm) and fixed for 10 min in 4% paraformaldehyde in PBS. Sections were permeabilized for 10 min in PBS + 0.1%–0.3%Triton (PBST) and blocked for 1 hr in 2.5% fish gelatin, 5% normal donkey serum, 0.5% BSA, 0.1%–0.3% Triton in PBS. Primary antibodies (Abs) were incubated overnight 4°C and secondary Abs were incubated 1–2 hr at RT. Mouse Abs were incubated with M.O.M. block according to manufacturer's directions.

Detection of β-Galactosidase Activity and In Situ Hybridization

Frozen sections (20 μm) were fixed with 0.5% glutaraldehyde in PBS for 2 min, washed with PBS, and then incubated with 1 mg/ml Xgal substrates in PBS with 1.3 mM $MgCl_2$, 3 mM $K_3Fe(CN)_6$, and 3 mM $K_4Fe(CN)_6$ for 1 hr at 37°C. In situ hybridization for *Shh* was performed essentially as described previously (DasGupta and Fuchs, 1999). The construct used to generate *Shh in situ* probe was a gift from Andrew McMahon (Echelard et al., 1993). In situ hybridization for *Gli1* (region: 25–1205) was performed using RNAscope assays according to the manufacturer's instructions (Advanced Cell Diagnostics).

FACS

Purification of $K6^+$ bulge was performed using K6-RFP, Lhx2-EGFP double-transgenic mice. Purification of ORS was performed using Lgr5-EGFP mice. The upper and lower ORS cells were differentiated based on differences in their α6 levels. For cell isolation, the backskin was placed dermis side down in Collagenase (Sigma) for 30 min–1 hr. The dermal fractions were collected by scraping the dermal side using a scalpel. The remaining epidermal side was then transferred to Trypsin (GIBCO) at 37°C for 20–30 min. Single-cell suspensions were obtained by scraping the skin gently. The cells were then filtered with strainers (70 μM, followed by 40 μM). Cell suspensions were incubated with the appropriate antibodies for 30 min at RT. The following antibodies were used: CD34-eFluor660 (1:100, eBioscience), α6-PE (1:500, eBioscience), β1-PE_Cy7 (1:250, eBioscience), Sca1-PerCP_Cy5.5 (1:1000, eBioscience), CD140a-PE (1:100, eBioscience), CD31-eFluor450 (1:100, eBioscience). CD45-eFluor450 (1:100, eBioscience), CD24-FITC (1:100, eBioscience), Pcad-Biotin (1:25, R&D), EphrinB1-Biotin (1:50 R&D), CD200-eFluor660 (1:100, eBioscience). DAPI was used to exclude dead cells. Cell isolations were performed on FACSAria sorters equipped with Diva software (BD Biosciences). FACS analyses were performed using LSRII FACS Analyzers and then analyzed with FlowJo program.

Real-Time PCR

Total RNAs were purified from FACS-sorted cells by directly sorting into Trizol^{LS} (Life Technologies) followed by extraction using Direct-Zol RNA mini-prep kit (Zymo Research). Equal amounts of RNA were reverse-transcribed by Oligo-dT (Superscript III, Life Technologies). cDNAs were normalized to equal amounts using primers against Ppib2 or β-actin.

Confocal Microscopy and Image Processing

Images were acquired with a Zeiss LSM510 or a Zeiss LSM780 laser-scanning microscope (Carl Zeiss MicroImaging) through a 40× water objective or a 25× objective. Representative single Z planes are presented and colocalizations were interpreted only in single Z

stacks. Z stacks were projected using ImageJ software. RGB images were assembled in Adobe Photoshop CS5, and panels were labeled in Adobe Illustrator CS5.

SUPPLEMENTAL REFERENCES

Bai, C.B., Auerbach, W., Lee, J.S., Stephen, D., and Joyner, A.L. (2002). Gli2, but not Gli1, is required for initial Shh signaling and ectopic activation of the Shh pathway. Development *129*, 4753–4761.

Corrales, J.D., Blaess, S., Mahoney, E.M., and Joyner, A.L. (2006). The level of sonic hedgehog signaling regulates the complexity of cerebellar foliation. Development *133*, 1811–1821.

DasGupta, R., and Fuchs, E. (1999). Multiple roles for activated LEF/TCF transcription complexes during hair follicle development and differentiation. Development *126*, 4557–4568.

Dassule, H.R., Lewis, P., Bei, M., Maas, R., and McMahon, A.P. (2000). Sonic hedgehog regulates growth and morphogenesis of the tooth. Development *127*, 4775–4785.

Echelard, Y., Epstein, D.J., St-Jacques, B., Shen, L., Mohler, J., McMahon, J.A., and McMahon, A.P. (1993). Sonic hedgehog, a member of a family of putative signaling molecules, is implicated in the regulation of CNS polarity. Cell *75*, 1417–1430.

Long, F., Zhang, X.M., Karp, S., Yang, Y., and McMahon, A.P. (2001). Genetic manipulation of hedgehog signaling in the endochondral skeleton reveals a direct role in the regulation of chondrocyte proliferation. Development *128*, 5099–5108.

Mao, X., Fujiwara, Y., and Orkin, S.H. (1999). Improved reporter strain for monitoring Cre recombinase-mediated DNA excisions in mice. Proc. Natl. Acad. Sci. USA *96*, 5037–5042.

Nguyen, H., Rendl, M., and Fuchs, E. (2006). Tcf3 governs stem cell features and represses cell fate determination in skin. Cell *127*, 171–183.

Srinivas, S., Watanabe, T., Lin, C.S., William, C.M., Tanabe, Y., Jessell, T.M., and Costantini, F. (2001). Cre reporter strains produced by targeted insertion of EYFP and ECFP into the ROSA26 locus. BMC Dev. Biol. *1*, 4.

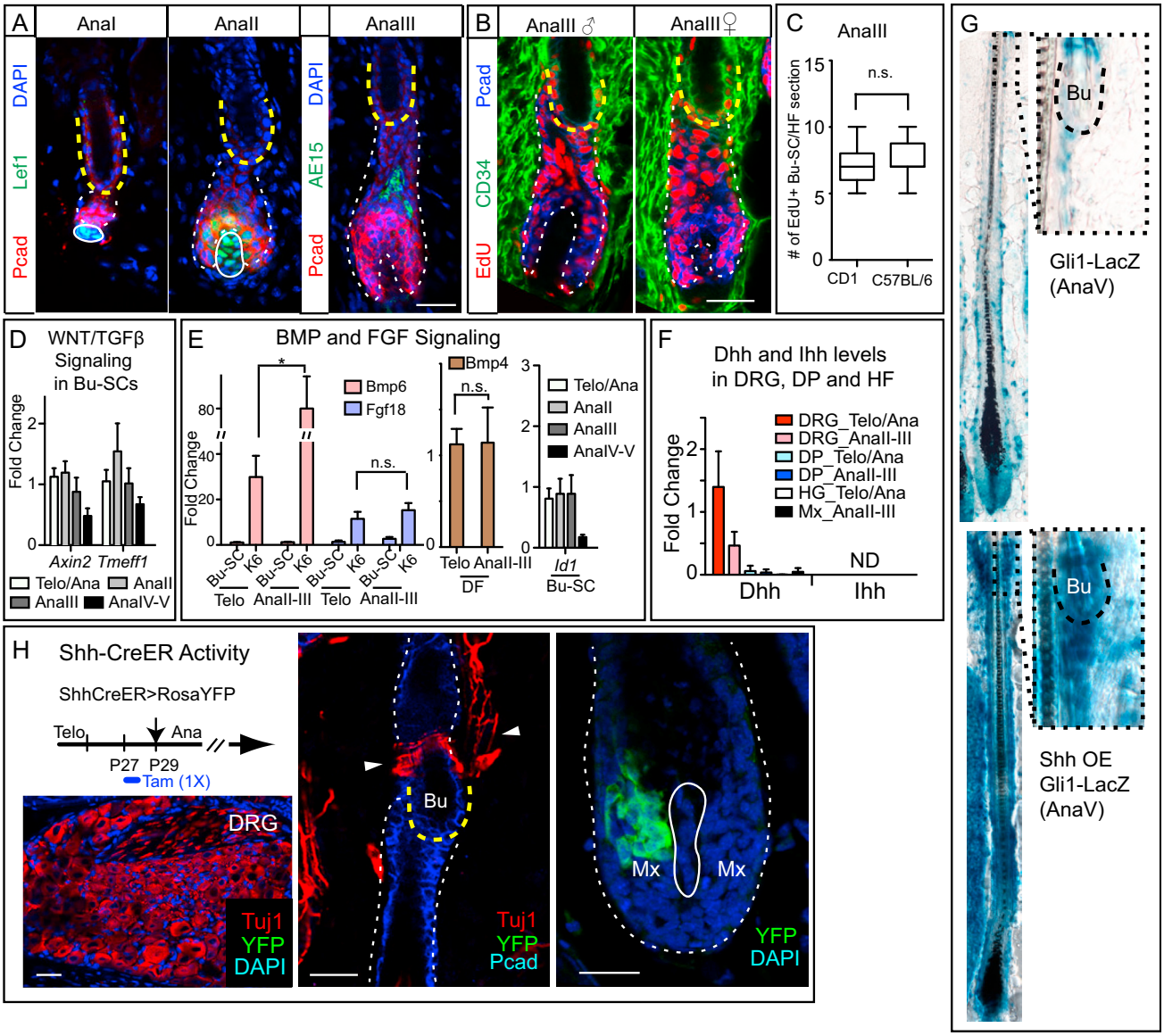

Figure S1. Early Anagen Markers, Bu-SC Activity across Strains and Sex, Signaling Activities within the Niche, and *Gli1-LacZ* Activity, Related to Figure 1

(A) Marker expression during early anagen. In AnaII, matrix cells (LEF1 and Pcad double positive) start to form at the bottom of the hair bulb, right on top of DP (LEF1 single positive). In AnaIII, differentiated IRS cells ($AE15^+$) begin to emerge.

(B) EdU incorporation in AnaIII HFs from male and female samples.

(C) Quantifications of EdU^+ Bu-SCs per bulge comparing outbred CD1 mice to inbred C57BL/6 mice at AnaIII (n = 3 for CD1; n = 2 for C57BL/6; ≥ 15 HFs per mice). n.s., not significant.

(D) RT-PCR results of *Axin2* (WNT signaling) and *Tmeff1* (TGF-β signaling) from purified Bu-SCs at different hair cycle substages.

(E) RT-PCR examining *Bmp6* and *Fgf18* levels in purified Bu-SCs and $K6^+$ bulge, *Bmp4* in dermal fibroblast (DF), and *Id1* (BMP signaling) in Bu-SCs.

(F) RT-PCR of *Dhh and Ihh* levels from dissected DRGs, FACS-purified DP, HG, or matrix at either telogen→anagen transition or at AnaII–III. *Ihh* was not detected (ND) in any of these cell types.

(G) β-gal activity (blue) of AnaV, *Gli1-LacZ* HF (Top) and AnaV, *Gli1-LacZ* HF with SHH overexpression (OE, bottom).

(H) Examining HFs, DRGs, and cutaneous nerve fibers for expression of YFP^+ cells 2 days after induction of *ShhCreER/ Rosa*$^{flox\text{-}stop\text{-}flox\text{-}YFP}$ with one injection of Tamoxifen (150 μg/g tamoxifen in corn oil).

Bulge, yellow dashed lines; the rest of the HF, white dashed lines. DP, solid line. Box-and-whisker plots: midline, median; box, 25th and 75th percentiles; whiskers, minimum and maximum. Scale bars, 30 μm. Data are mean ± SD n.s., not significant. *$p < 0.05$.

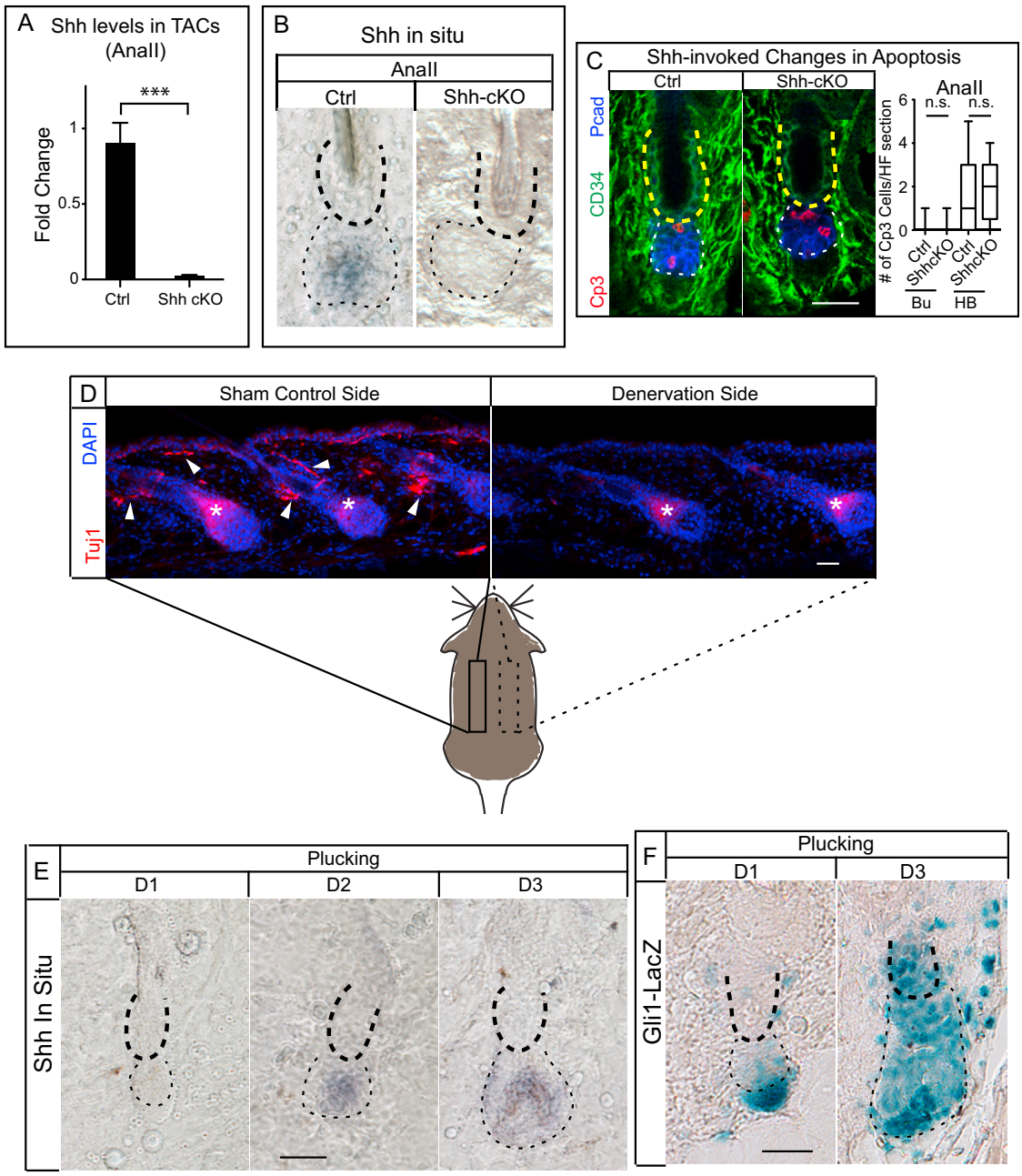

Figure S2. *Shh*, *Shh* Signaling Levels, and Apoptosis Analysis in Control and *Shh*-cKO HFs and the Design of the Denervation Scheme, Related to Figure 2

(A) RT-PCR of *Shh* in purified hair bulb from control and *Shh*-cKO HFs at AnaII.

(B) In situ hybridization of *Shh* in control and *Shh*-cKO HFs at AnaII.

(C) Immunolocalization of active Caspase 3 (Cp3), CD34 and Pcad in control and *Shh*-cKO HFs and quantifications.

(D) Schematic and low power view to demonstrate the design and efficiency of the denervation surgery. An incision was made at the midline and nerve fibers were manually removed by a spring scissor only at the right side of the skin (Denervation Side). The connective tissues were also cleaned by a scissor but the nerves were not cut at the left side (Sham Control Side). Arrowheads mark the Tuj1$^+$ cutaneous nerve fibers, which are intact at the control side but are absent at the denervation side. Asterisks mark the Tuj1$^+$ IRS cells, which are present at both sides. The HFs on both sides are in AnaIII.

(E) In situ hybridization detecting *Shh* expression in HFs at different time points after plucking during telogen. HFs are plucked at D0. *Shh* expression is absent at D1 after plucking but becomes detectable starting from D2.

(F) β-gal activity of *Gli1-LacZ* HFs at D1 and D3 post-plucking.

Bulge: thick dashed lines or yellow dashed lines. Hair bulbs: thin dashed lines or white dashed lines. Scale bars, 30 μm.

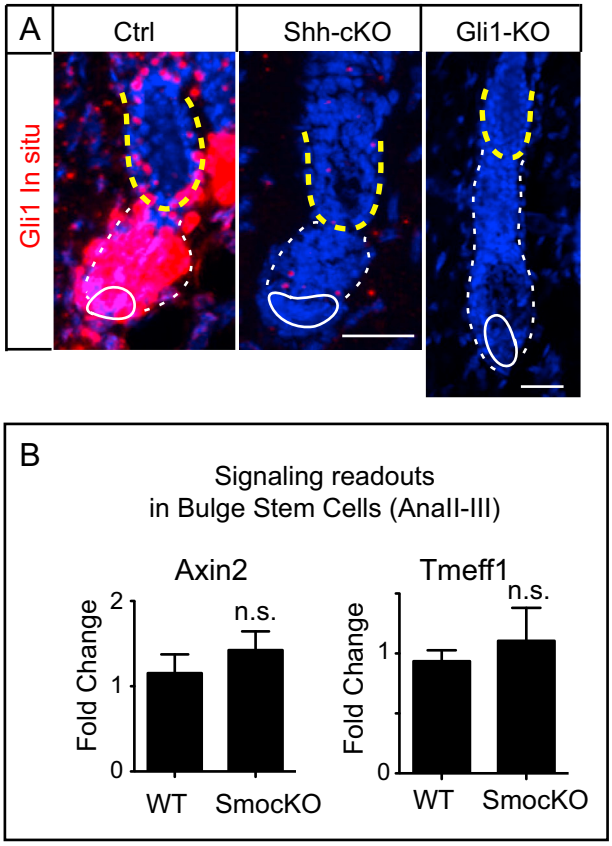

Figure S3. *Gli1* In Situ Hybridization and Gene-Expression Analysis in *Smo*-cKO, Related to Figure 3

(A) In situ hybridization of *Gli1* in control, *Shh*-cKO, and *Gli1* KO HFs. Bulge, yellow dashed lines; the rest of the HF, white dashed lines. DP, solid lines.

(B) RT-PCR results of WNT signaling target *Axin2* and TGF-β signaling target *Tmeff* in FACS-purified WT or *Smo-cko* Bu-SCs in AnaII–III. Both pathways operate normally in Bu-SCs when they are defective of SHH pathway activity.

Data are mean ± SD n.s., not significant.

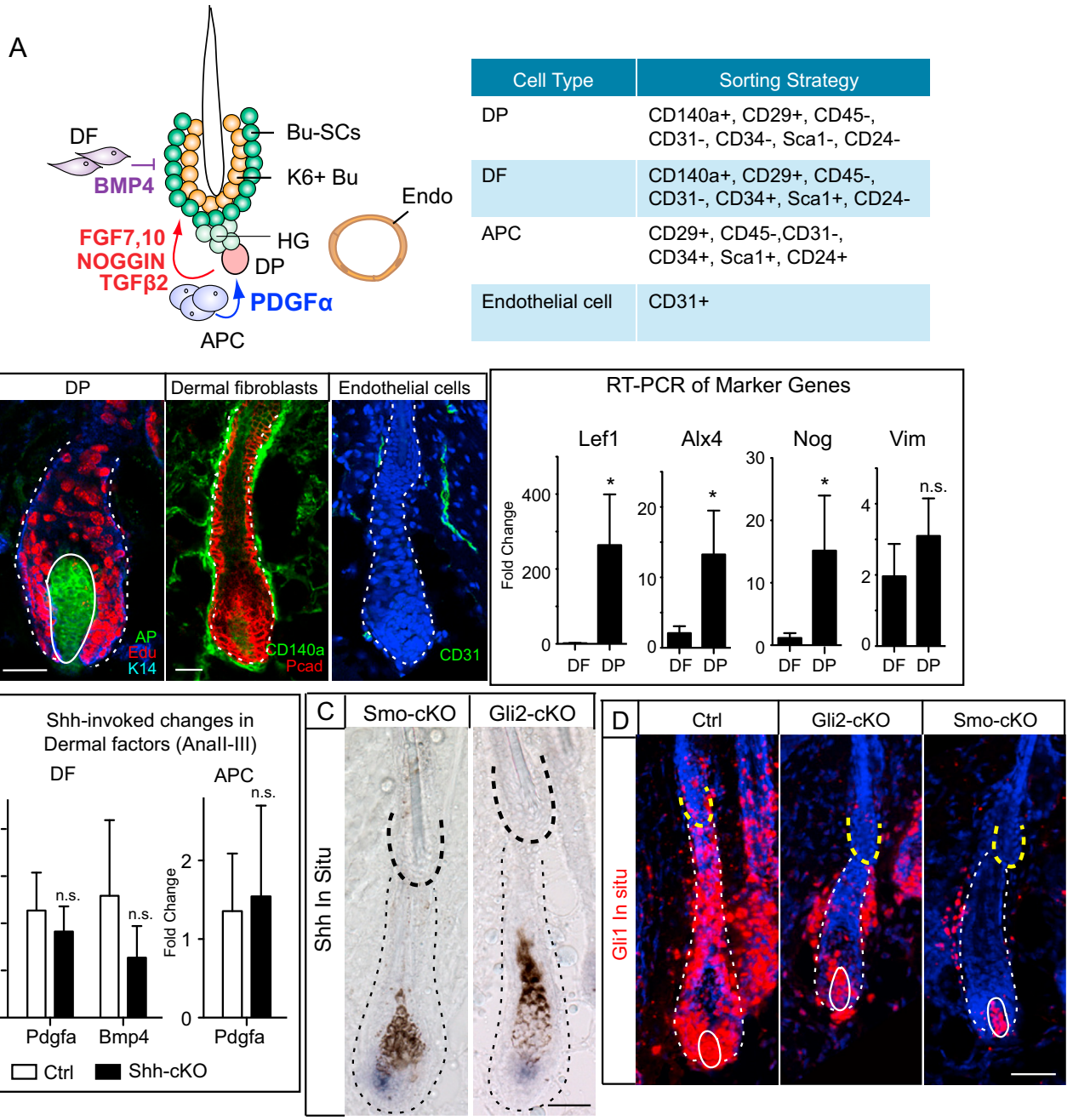

Cell Type	Sorting Strategy
DP	CD140a+, CD29+, CD45-, CD31-, CD34-, Sca1-, CD24-
DF	CD140a+, CD29+, CD45-, CD31-, CD34+, Sca1+, CD24-
APC	CD29+, CD45-,CD31-, CD34+, Sca1+, CD24+
Endothelial cell	CD31+

Figure S4. Isolation Strategies and Gene-Expression Analysis for Various Dermal Cell Types, Related to Figure 4

(A) Isolation strategies employed to enrich for dermal cell types including DP (dermal papillae), DF (dermal fibroblasts), APC (adipocyte precursor cells), and Endo (endothelial cells). (Top) Schematic representation of dermal cell types that are in close proximity to the HFs and surface markers used to enrich for various dermal cell types. (Bottom left) Immunolocalization of markers for different dermal cell types revealing their relative positions to a HF. HF, white dashed lines. DP, solid line. (Bottom right) RT-PCR of signature genes verifies the successful enrichment of DP from DF. *Lef1*, *Alx4*, and *Nog* are known DP signatures, whereas *Vimentin* (*Vim*) is expressed by both the DP and DF.

(B) RT-PCR examining gene expression in purified dermal cell types from WT and *Shh-cKO* skin enriched for AnaII and AnaIII HFs.

(C) In situ hybridization of *Shh* in *Smo*-cKO and *Gli2*-cKO HFs. Bulge: thick dashed lines. Hair bulbs: thin dashed lines.

(D) In situ hybridization of *Gli1* in control, *Gli2*-cKO, and *Smo*-cKO HFs. Bulge, yellow dashed lines; the rest of the HF, white dashed lines. DP, solid lines. Scale bars, 30 μm. Data are mean ± SD. *$p < 0.05$. n.s., not significant.

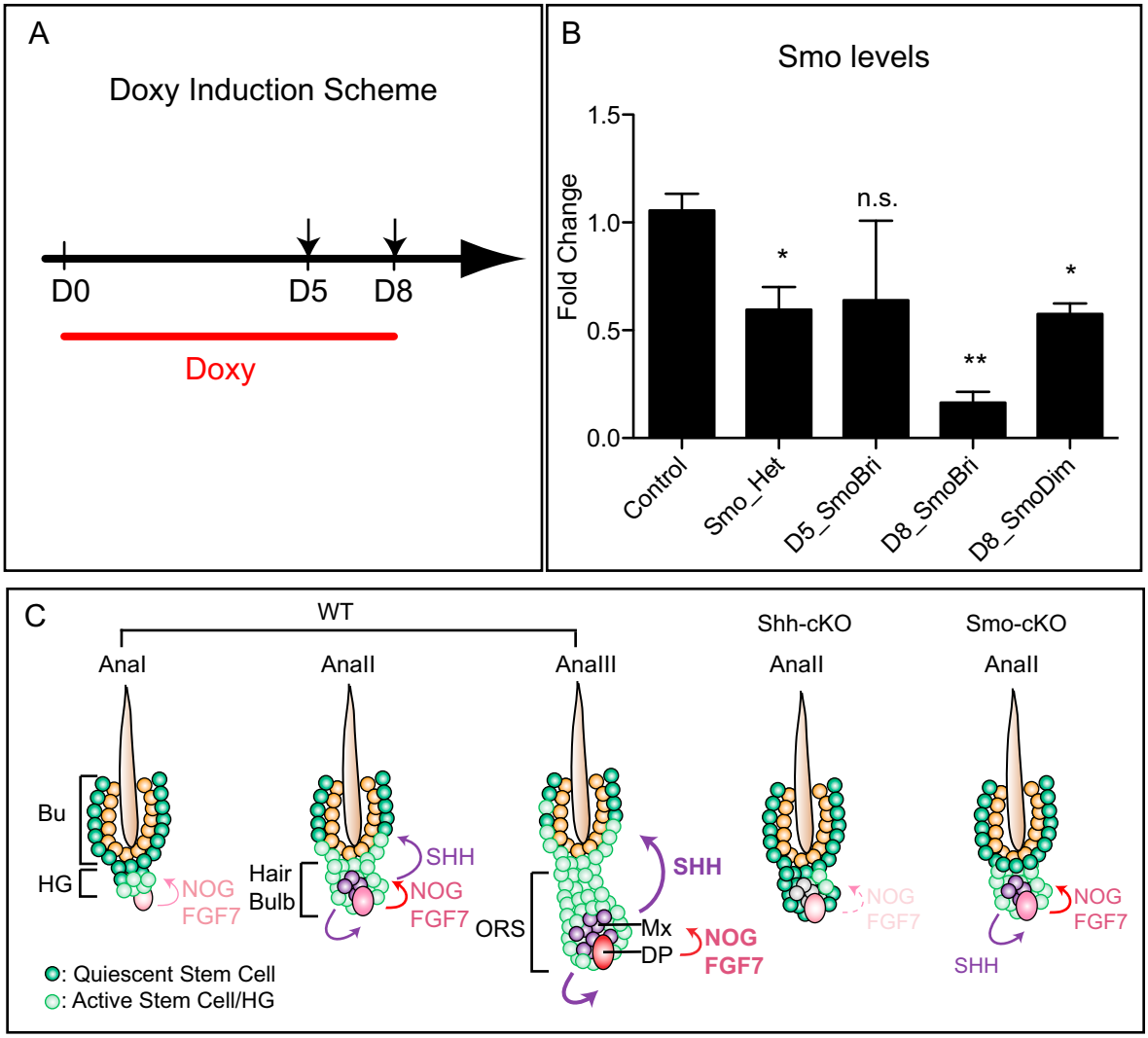

Figure S5. Efficiency of *Smo*-Inducible Knockdown, Related to Figure 5

(A) Schematic summarizes the design of Doxycycline (Doxy) induction scheme for testing hairpin efficiency in vivo. Mice are fed with Doxy chow starting at D0, and knockdown efficiency was examined at D5 and D8 in FACS-purified Bu-SCs.

(B) RT-PCR examining *Smo* expression levels in FACS-purified Bu-SCs from control, Smo^{het}, and skins infected with *Smo* hairpins (SmoBri: RFP^{Bright} *Smo* knockdown cells; SmoDim: RFP^{Dim} *Smo* knockdown cells). RFP^{Dim} *Smo* knockdown cells have comparable *Smo* expression levels to Smo^{het} cells, which resemble wild-type phenotypically. Data are mean ± SD. *$p < 0.05$; **$p < 0.01$. n.s., not significant.

(C) Model summarizing direct and indirect requirement of SHH in Bu-SCs and hair bulb proliferation during early anagen.

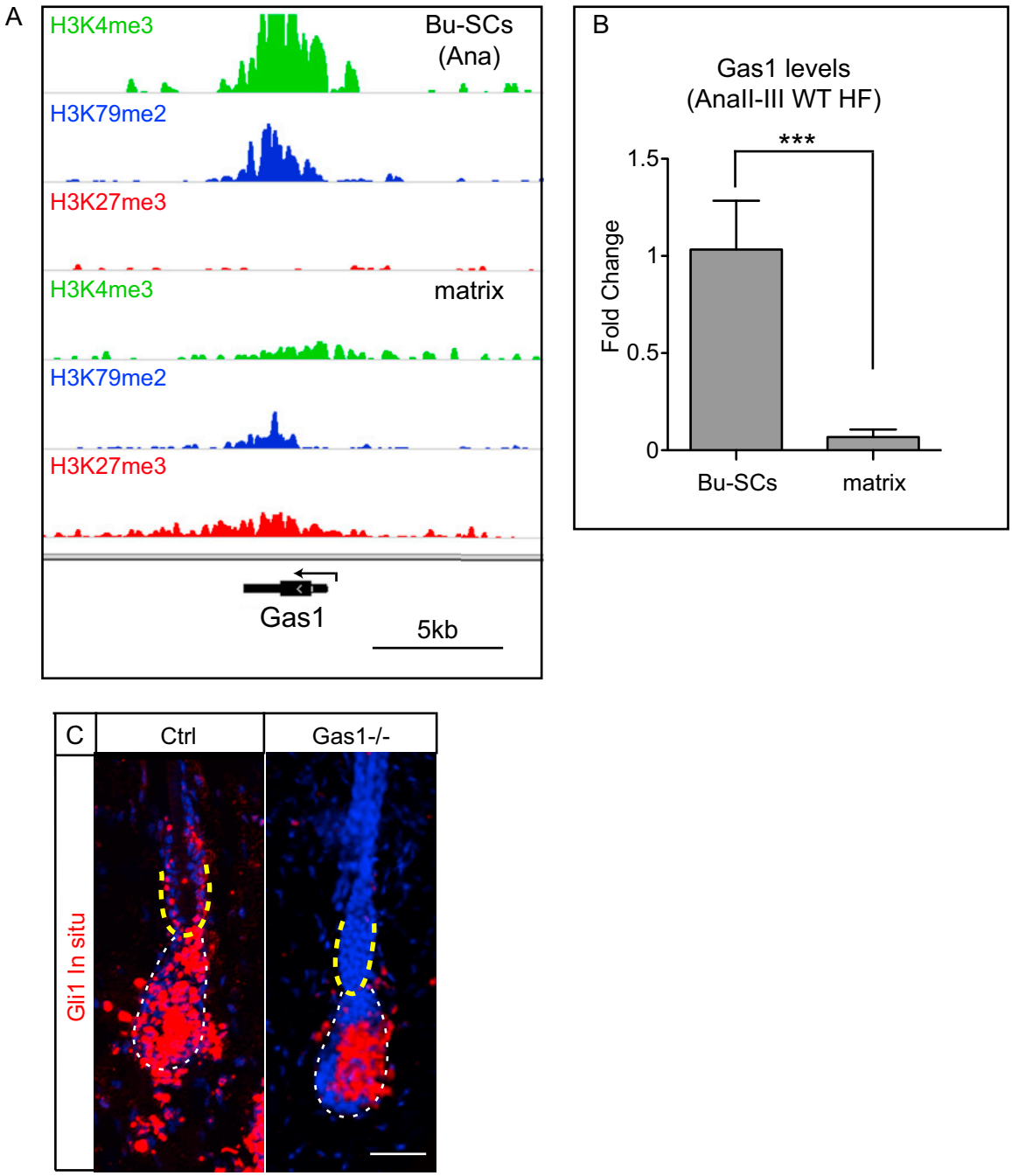

Figure S6. *Gas1* Expression in Bu-SCs and Matrix and *Gli1* Levels in *Gas1*$^{-/-}$, Related to Figure 6

(A) ChIP-seq signal tracks around the *Gas1* locus. Chromatin is from anagen Bu-SCs and TAC matrix. Antibodies bind to H3 modifications of different transcriptional events including initiation (lysine 4 trimethylation, H3K4me3), elongation (lysine 79 dimethylation, H3K79me2), and dominant repression (lysine 27 trimethylation, H3K27me3). *Gas1* is highly and actively transcribed in the anagen Bu-SCs, but is repressed in the TAC matrix. All tracks are shown on the same scale.

(B) RT-PCR testing *Gas1* levels in purified Bu-SCs and matrix from HFs enriched at AnaII–III. Data are mean ± SD. ***p < 0.001.)

(C) In situ hybridization of *Gli1* in control and *Gas1*$^{-/-}$ HFs. Bulge, yellow dashed lines; the rest of the HF, white dashed lines. Scale bars, 30 μm.

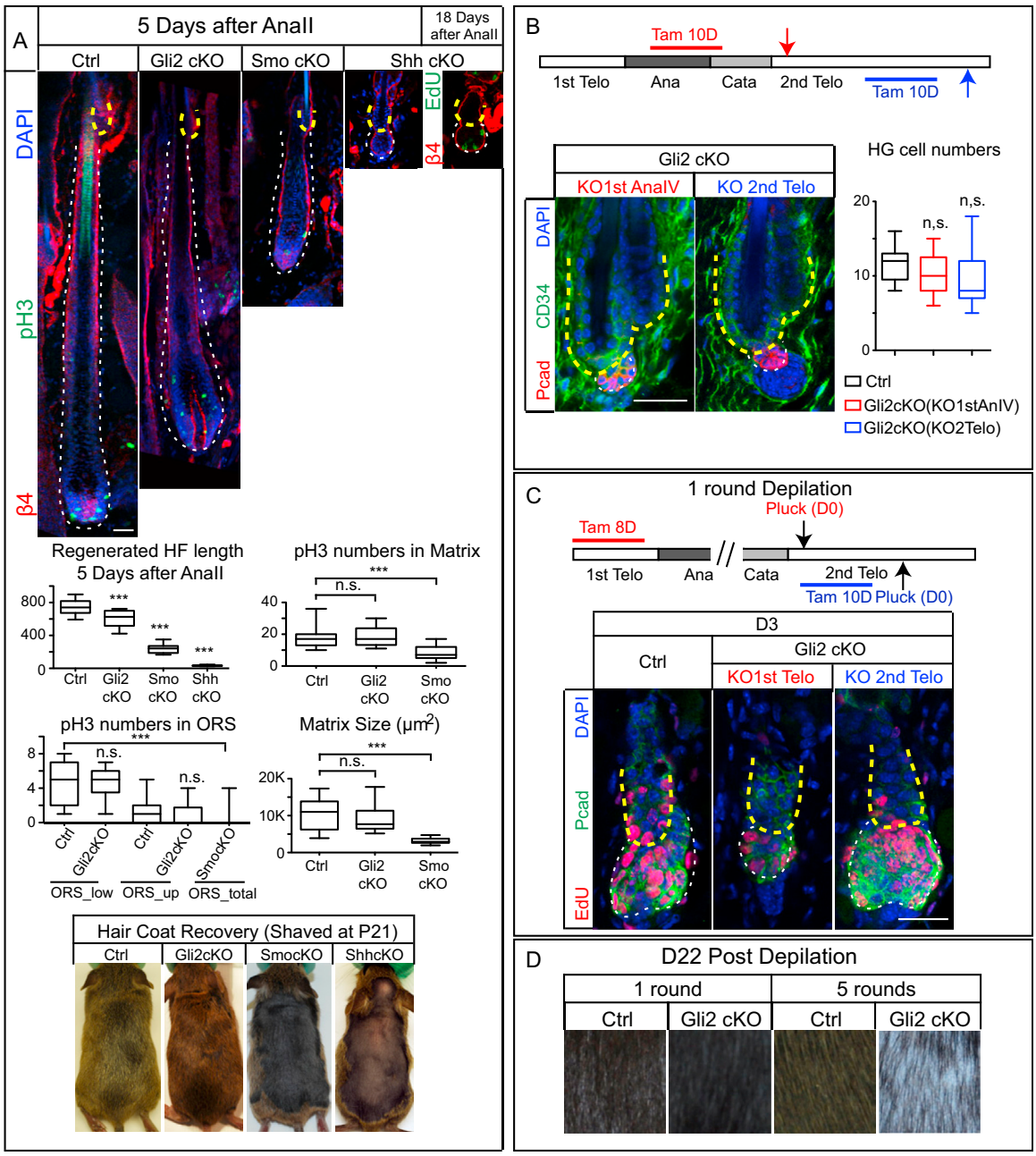

Figure S7. *Shh* Pathway Mutants in Full Anagen and *Gli2*-cKO Phenotypes, Related to Figure 7

(A) (Top) Control, *Gli2*-cKO, *Smo*-cKO, and *Shh*-cKO HFs 5 days after AnaII and *Shh*-cKO HFs 18 days after AnaII. (Middle) Quantifications of regenerated HF length below bulge, proliferation status (measured by pH3, phospho-Histone H3), and matrix size. Note that proliferation status of matrix and ORS was measured by pH3 staining instead of EdU, as EdU incorporation becomes saturated rapidly in highly proliferative populations like matrix and lower ORS, which often leads to an underestimation of proliferation differences. (Bottom) Representative pictures of hair coat recovery of different SHH pathway mutants. The mice were shaved in P21, and photos were taken between P55–P62, when all littermate controls had recovered their hair coat completely.

(B) 2nd telogen HFs with *Gli2* knocked out at different time points and quantifications of their HG sizes compared to those of the control. *Gli2* is knocked out either in 1st AnaIV, when Bu-SCs return to quiescence (red bars) or 2nd telogen (blue bars).

(C) Representative images of control and *Gli2*-cKO mice with one round of hair plucking. *Gli2* is knocked out either in 1st telogen or 2nd telogen.

(D) Close up pictures of skin surface in control and *Gli2*-cKO animals after 1 round or 5 rounds of hair depilation. *Gli2* is knocked out since 1st telogen.

Bulge, yellow dashed lines; the rest of the HF, white dashed lines. Box-and-whisker plots: midline, median; box, 25th and 75th percentiles; whiskers, minimum and maximum. Scale bars, 30 μm. n.s., not significant. ***$p < 0.001$.